2018

First U-Pb zircon ages for late Miocene Ashfall *Konservat-Lagerstatte* and Grove Lake ashes from eastern Great Plains, USA

Jon J. Smith
Kansas Geological Survey, jjsmith@ku.edu

Elijah Turner
University of Kansas

Andreas Moller
University of Kansas

Robert M. Joeckel
University of Nebraska - Lincoln, rjoeckel3@unl.edu

Rick E. Otto
University of Nebraska - Lincoln, rick.otto@unl.edu

PLOS ONE

RESEARCH ARTICLE

First U-Pb zircon ages for late Miocene Ashfall *Konservat-Lagerstätte* and Grove Lake ashes from eastern Great Plains, USA

Jon J. Smith[1]*, Elijah Turner[2], Andreas Möller[2], R. M. Joeckel[3], Rick E. Otto[4]

1 Kansas Geological Survey, Lawrence, KS, United States of America, **2** The University of Kansas, Department of Geology, Lawrence, KS, United States of America, **3** Conservation and Survey Division, School of Natural Resources and Department of Earth and Atmospheric Sciences, University of Nebraska-Lincoln, Hardin Hall, Lincoln, NE, United States of America, **4** University of Nebraska–Lincoln, University of Nebraska State Museum, Lincoln, Nebraska, United States of America, and Ashfall Fossil Beds, University of Nebraska State Museum, Royal, Nebraska, United States of America

* jjsmith@ku.edu

Citation: Smith JJ, Turner E, Möller A, Joeckel RM, Otto RE (2018) First U-Pb zircon ages for late Miocene Ashfall *Konservat-Lagerstätte* and Grove Lake ashes from eastern Great Plains, USA. PLoS ONE 13(11): e0207103. https://doi.org/10.1371/journal.pone.0207103

Editor: Alex Dickson, Royal Holloway University of London, UNITED KINGDOM

Received: August 2, 2018

Accepted: October 24, 2018

Published: November 8, 2018

Data Availability Statement: All relevant data are within the manuscript and its Supporting Information files.

Funding: Author JJS received funding from the National Science Foundation, Directorate for Geosciences, Grant EAR-1023285 (https://www.nsf.gov/). The funders had no role in study design, data collection and analysis, decision to publish, or preparation of the manuscript.

Competing interests: The authors have declared that no competing interests exist.

Abstract

This paper documents the first U-Pb zircon ages for Ashfall Fossil Beds (Nebraska, USA), a terrestrial *Konservat-Lagerstätte* mass-death assemblage that is arguably the most diverse of its type and age. The Ashfall tephra was correlated with ignimbrites from the Bruneau-Jarbidge volcanic field (12.7–10.5 Ma) in southwest Idaho based on geochemical analysis. The methods and geochemical data supporting the original age assessment of the ash bed, however, were never published, and there has been a persistent misconception that dateable heavy minerals (e.g., zircon) are absent. Notwithstanding, we recovered abundant zircons from Ashfall Fossil Beds, and from an ash bed ~6 km to the southeast at Grove Lake, Nebraska, and analyzed them through LA-ICP-MS. Our new zircon U-Pb age of 11.86 ± 0.13 Ma substantiates correlation of the Ashfall Fossil Beds deposit to tuffs originating from the Bruneau-Jarbidge caldera (~12.7–10.5 Ma). Our U-Pb zircon age of 6.42 ± 0.06 Ma for the Grove Lake ash bed coincides with supervolcanic activity in the Heise volcanic field (6.6–4.3 Ma) in eastern Idaho. These new dates improve age constraints of strata comprising the Ogallala Group and the important paleontological site. Moreover, we find that detrital and airfall zircons are unevenly distributed in the stratified ash beds we describe herein and presumably in similar deposits worldwide. Therefore, a higher-resolution sampling scheme is necessary in such cases.

Introduction

Ashfall Fossil Beds State Historical Park (Fig 1), a U.S. National Natural Landmark, is a terrestrial *Konservat-Lagerstätte* mass-death assemblage composed of Miocene amphibians, reptiles, birds, and mammals within an ~3-m-thick vitric ash deposit [1, 2]. The area encompassing Ashfall Fossil Beds has been the focus of nearly continuous paleontological research since its discovery in the early 1950's (e.g. [1, 2, 3, 4, 5, 6, 7, 8, 9, 10, 11]). In recent decades, Ashfall is frequently associated in the popular press (e.g. [12]) with the concerns regarding the scale and potential impacts of Yellowstone supervolcanic eruptions (ejecta volumes >100 km^3) [13].

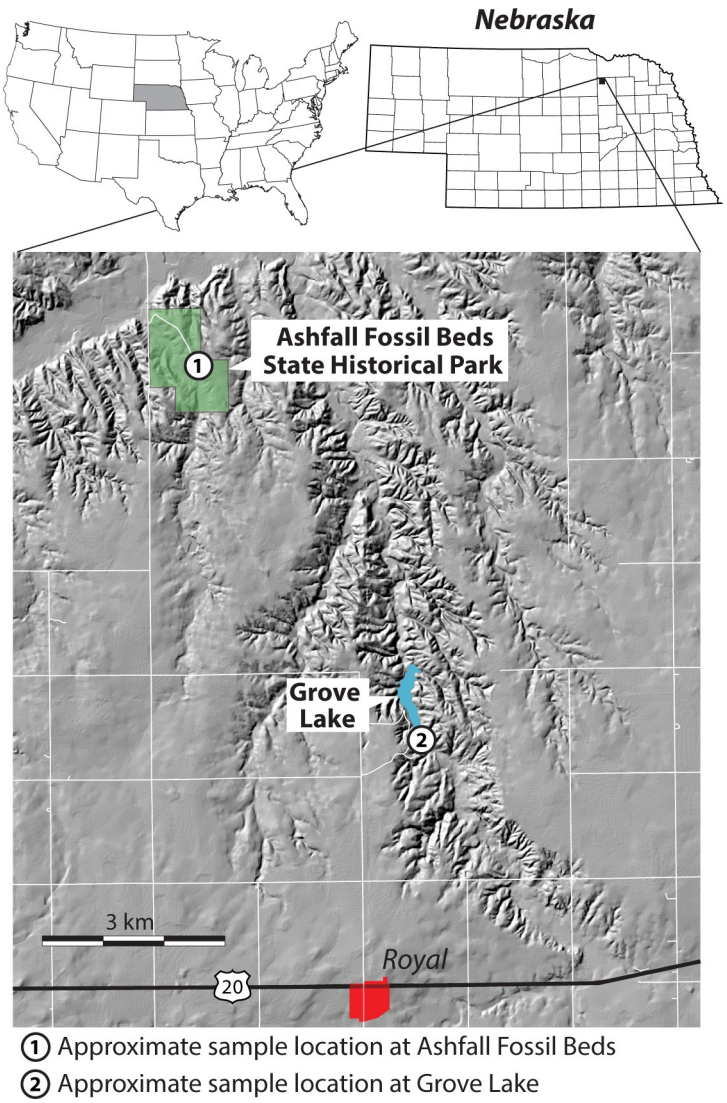

Fig 1. Location of study areas of Ashfall Fossil Beds State Historical Park and Grove Lake, Nebraska. Base map is DEM hillshade downloaded from the from USGS National Map Viewer (open access) at https://viewer.nationalmap.gov/viewer/.

https://doi.org/10.1371/journal.pone.0207103.g001

Ash beds, and K-bentonites as their weathered equivalents, are critical geochronological marker horizons because tephrochronologic correlations or the radiometric dating of volcanic minerals of airfall tephra constrain the depositional ages of host strata and are significant for the development of a regional chronostratigraphy (e.g. [14]). Tephrochronology is a geochemical technique that correlates distal ashfall deposits to well-dated proximal volcanic tuffs through the electron probe microprobe analysis of glass shards (e.g. [15, 16, 17]). Conventional wisdom maintains that preferred phenocrysts for the direct radiometric dating of ash beds, such as zircon and sanidine, are often rare or absent in distal airfall deposits [17].

Until the present paper, there have been no absolute ages published from Ashfall Fossil Beds. The bulk-glass chemistry of the ash correlates with ignimbrites of the Bruneau-Jarbidge volcanic field of the Snake River Plain in southeastern Idaho [18, 19, 20, 21]. This attribution is plausible because the *Lagerstätte* has been assigned to the Clarendonian North American Land

Mammal Age, which spans 13.6 to 10.3 Ma [2, 22], and which overlaps the span of active volcanism (12.7–10.5 Ma) in the Bruneau-Jarbidge field [16]. Information regarding the tephrochronologic correlation of the Ashfall tephra to tuffs from the Bruneau-Jarbidge caldera, however, was disseminated primarily through personal communications (see [2]), conference presentations and abstracts [18, 19, 21], and popular media reporting (e.g. [12, 20, 23, 24, 25]). In no way do we criticize past researchers in underscoring these points. Rather, we amplify their work through a different approach to dating, for which we describe rigorous specific methods and data supporting tephrochronologic correlations, thereby certifying the age of the ash and its *Lagerstätte* with the first directly measured absolute age at the site.

We conducted a direct test of the age of the Ashfall *Lagerstätte* by collecting samples from four superposed stratigraphic intervals at Ashfall and another four from an ash bed cropping out ~6 km to the southeast at Grove Lake (Fig 1). Zircon, sanidine, and other minerals used for dating volcanoclastic sediments were hitherto assumed to be absent from the fine-grained vitric ash deposit [2]. Processing our samples with standard mineral separation techniques, however, yielded abundant zircon crystals in the lowermost sampled intervals at both locations. We dated these zircon crystals through laser ablation inductively coupled mass spectrometry (LA-ICP-MS) and obtained U-Pb ages of eruption. Ages of eruption are identical to deposition within the limits of reproducibility of the technique (1–2%) [26]. Our new U-Pb ages are a significant step in the development of a chronostratigraphic framework of Cenozoic deposits in the Great Plains of North America. Furthermore, our research indicates that detrital and airfall zircons are not distributed evenly in stratified ash beds, particularly in reworked deposits, and that finding such grains may require a higher-resolution sampling scheme than is typically used.

Geologic background

The ash deposits exposed at Ashfall Fossil Beds State Historical Park and Grove Lake are both within the Miocene Ash Hollow Formation of the Ogallala Group (Fig 2) [2, 27, 28]. The Ogallala Group (Ogallala Formation outside of Nebraska) underlies much of the North American High Plains and consists chiefly of fluvial sand, sandstone, silt, and siltstone, with minor eolian sediments and local lenses of volcanic ash, and lacustrine limestones and diatomites [29, 30]. The Ogallala Group is composed of several formations in Nebraska [31, 32], but only the Valentine and Ash Hollow Formations, which comprise most of it, are recognized in the immediate vicinity of Ashfall Fossil Beds [23, 31, 33, 34, 35]. The Ashfall *Konservat-Lagerstätte*, is in the Cap Rock Member of the Ash Hollow Formation. The ash bed exposed at the nearby Grove Lake lies within the overlying Merritt Dam Member of the same formation (Fig 2).

The ash bed at Ashfall Fossil Beds is interpreted as the fill of a small depression on the basis of its lenticular geometry and the taphonomy and paleoecology of the *Lagerstätte*. Indeed, many volcanic ash beds in continental successions are swale-filling deposits having limited lateral extents [17, 28]. The remains of fossil diatoms and such small aquatic vertebrates as salamanders, frogs, and turtles [2, 9], in addition to the high concentration of mammalian fossils, suggests that the Ashfall site was a transient watering hole at the time of ash deposition. Seasonally dry subtropical savannas extended across Nebraska in the Miocene with year-round above freezing temperatures, as indicated by the presence of large tortoises [36, 37]. We interpret the younger Grove Lake ash as a depression fill as well.

Paleontology

The Ashfall Fossil Beds contains an extraordinary terrestrial *Konservat-Lagerstätte* of Miocene vertebrates in a mass death assemblage (Fig 3) [6]. The *Lagerstätte* is composed of 21 fossil taxa

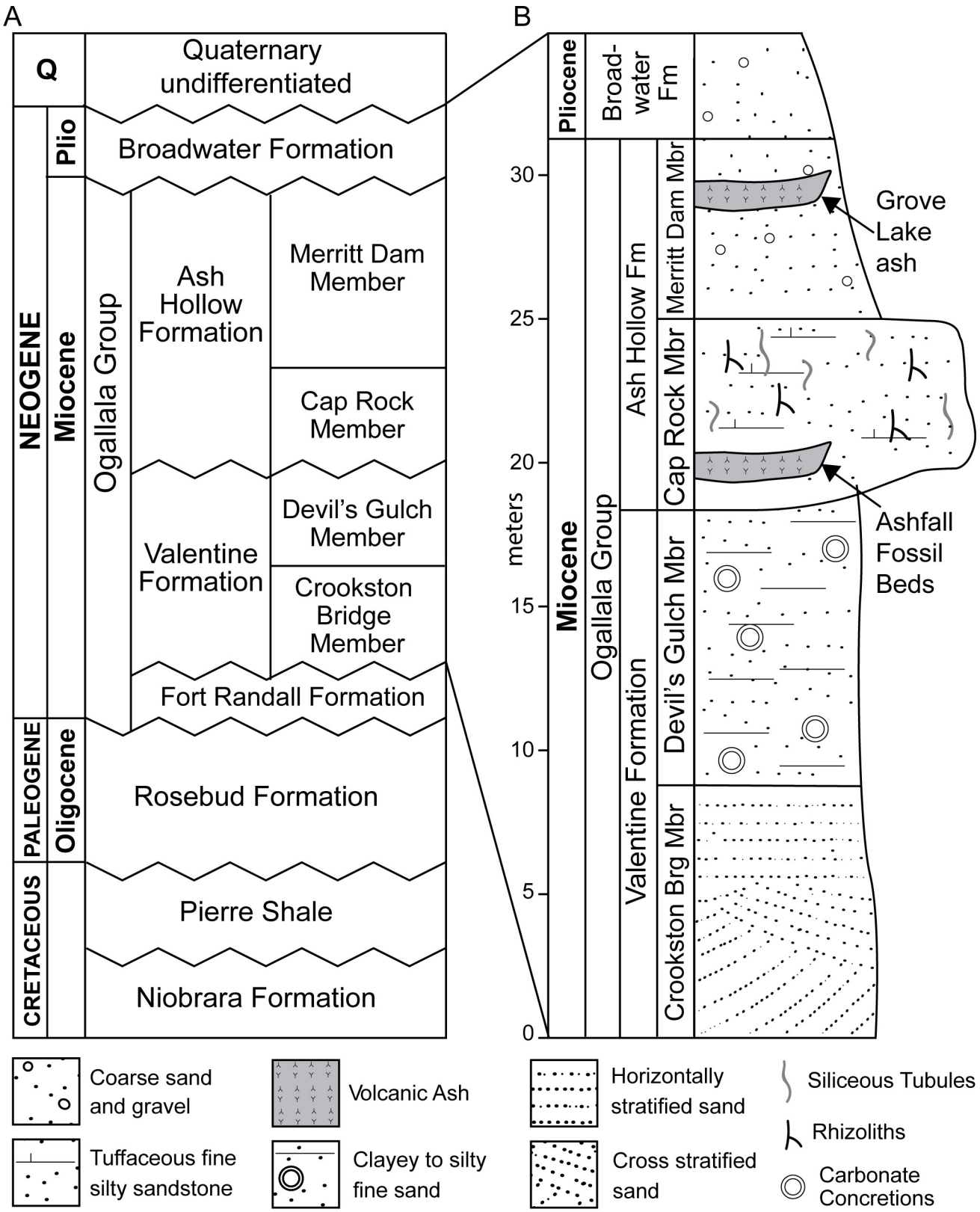

Fig 2. Stratigraphy of northern Antelope County, Nebraska. (A) Distribution of Cretaceous and Cenozoic strata in northeastern Nebraska. (B) Composite stratigraphic section of units exposed at the Ashfall site and Grove Lake. Modified from Voorhies [1] and Tucker et al. [2].

https://doi.org/10.1371/journal.pone.0207103.g002

representing amphibians, reptiles, birds, and mammals of the Clarendonian NALMA (13.6–10.3 Ma) in north-central Nebraska [2, 23]. The most numerous and well-known fossil remains are those of the barrel-bodied rhinoceros, *Teleoceras major* (Perissodactyla, Rhinocerotidae). Over 100 specimens of *T. major* have been uncovered in the tephra deposit, and it is hypothesized that most or all were members of a single social group [8]. Many of the medium- to large-sized mammal skeletons are fully articulated and preserved in their original three-dimensional death poses.

The mass mortality *Lagerstätte* was the direct result of volcanic ash deposition, though several taphonomic lines of evidence suggest that medium- to large-sized ungulates succumbed to long-term ash exposure, as opposed to a single catastrophic burial event [2]. The first line of evidence is that the fossil taxa within the *Lagerstätte* are distributed vertically into three distinct and superposed assemblages separated by ~10–15 cm of unfossiliferous ash (Fig 3A). The base of the ash bed contains the mostly fragmentary remains of such relatively small animals as

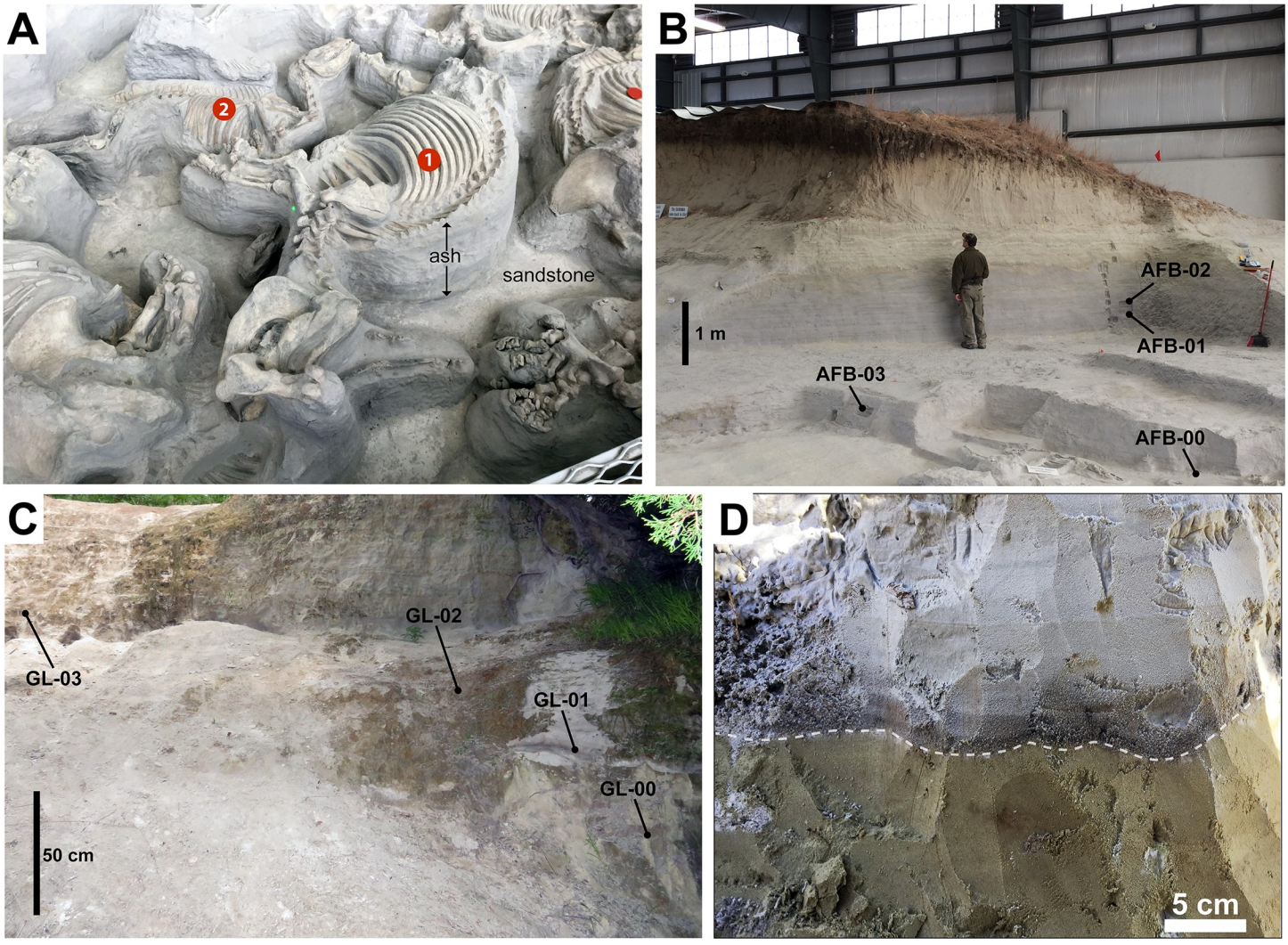

Fig 3. Outcrop photographs of the Ashfall Fossil Beds and Grove Lake ash localities. (A) Ashfall *Konservat-Lagerstätte* from inside the Hubbard Rhino Barn showing ash pillars supporting (1) fully articulated fossils of Teleoceras major and (2) underlying medium-sized equid. (B) Ash bed in the Cap Rock Member exposed in the Hubbard Rhino Barn at Ashfall Fossil Beds showing sample locations for this study. (C) Ash bed in the Merritt Dam Member just west of Grove Lake and sample locations for this study. (D) Photograph of the dark colored basal horizon at Ashfall that contains dateable volcanogenic zircons (immediately above dotted line).

https://doi.org/10.1371/journal.pone.0207103.g003

turtles and wading birds. The second fossiliferous horizon contains medium-sized taxa, including several species of camelids and equids. The third assemblage, ~25 cm from the base of the ash bed, is composed mostly of fully articulated *Teleoceras major* skeletons. The vertical distribution of the fossil taxa suggests successive die-offs according to different body sizes and abilities to withstand exposure to the ash. The second line of evidence suggesting that the larger vertebrates survived the initial airfall event, at least in the short-term, is abnormal growths on the bones of equids, camelids, and rhinos that resemble hypertrophic osteopathy or Marie's disease [7]. Hypertrophic osteopathy is a bone pathology in mammals secondary to severe pulmonary diseases and inhalation of foreign objects [38]. These growths indicate that the larger ungulates succumbed only after several weeks or months of exposure to the ash after the initial airfall event.

Airfall tephra and tephrochronologic correlations

The Snake River Plain is an ~770 km long, northeast-southwest trending linear depression that extends primarily across southern Idaho (Fig 4A) and contains seven major volcanic provinces that are progressively younger toward the northeast [39, 40, 41]. These include, from west to east, the McDermitt, Owyhee-Humboldt, Bruneau-Jarbidge, Twin Falls, Picabo, Heise, and Yellowstone Plateau volcanic fields [16]. Volcanism in this region began ca. 16.6 Ma near the Nevada-Oregon border with an outpouring of flood basalts on the Columbia Plateau and the formation of rhyolitic eruptive centers further south [16]. In Neogene strata of the Great Plains, volcanic ashes from the Snake River Plain volcanic province are preserved as airfall tephra composed primarily of fine-grained micron-scale rhyolitic glass bubble-wall shards sorted by long-distance atmospheric transport [42].

Proximal tuffs within the Bruneau-Jarbidge volcanic field range in age from ~12.7–10.5 Ma and are correlated regionally to distal airfall deposits in Idaho, Nevada, California, Colorado, New Mexico and throughout the Great Plains (Fig 4B) [16, 17, 43, 44, 45, 46, 47]. Total cumulative eruptive volume from Bruneau-Jarbidge is estimated to be 10^4–14^4 km^3 [16, 48]. If an estimated 30% of this mass was dispersed as airfall ash [49], the largest individual eruption events at Bruneau-Jarbidge were potentially capable of producing over 1000 km^3 of distal airfall deposits [48].

In a published abstract, Perkins [19] tentatively correlated the Ashfall Fossil Beds tephra with a tuff within the Bruneau-Jarbidge volcanic field, the Ibex Hollow Tuff (11.93 Ma). According to Perkins and Nash (see fig 5 in [16])], at least 22 Miocene-age tuffs of the Snake River Plain can be tephrochronologically correlated to ashes on the Great Plains, though the authors did not report the locations and stratigraphic positions of these distal ashes. Dobbins [50] made a tentative geochemical correlation of the Ashfall deposit to a Bruneau-Jarbidge eruption, the 10.45 ± 0.10 Ma Cougar Point Tuff XV, and concluded that the Ashfall deposit likely resulted from a single eruption event.

Materials and methods

We collected eight bulk sediment samples from ash beds located at Ashfall Fossil Beds (42.420, -98.156) and nearby Grove Lake (42.375, -98.119) for analysis. We obtained permission to access and sample study co-author, Rick E. Otto, park superintendent of Ashfall Fossil Beds State Historical Park. Four volcanic ash samples were collected inside the Hubbard Rhino Barn at Ashfall Fossil Beds State Historical Park (Fig 3B). A second set of four ash samples was collected approximately 6 km southeast of Ashfall Fossil Beds from an ash bed near Grove Lake (Fig 3C). At both locations, approximately 4-liters of ash were collected from four discrete stratigraphic intervals (Fig 5A and 5B). The outermost 5–8 cm of the outcrop was scraped

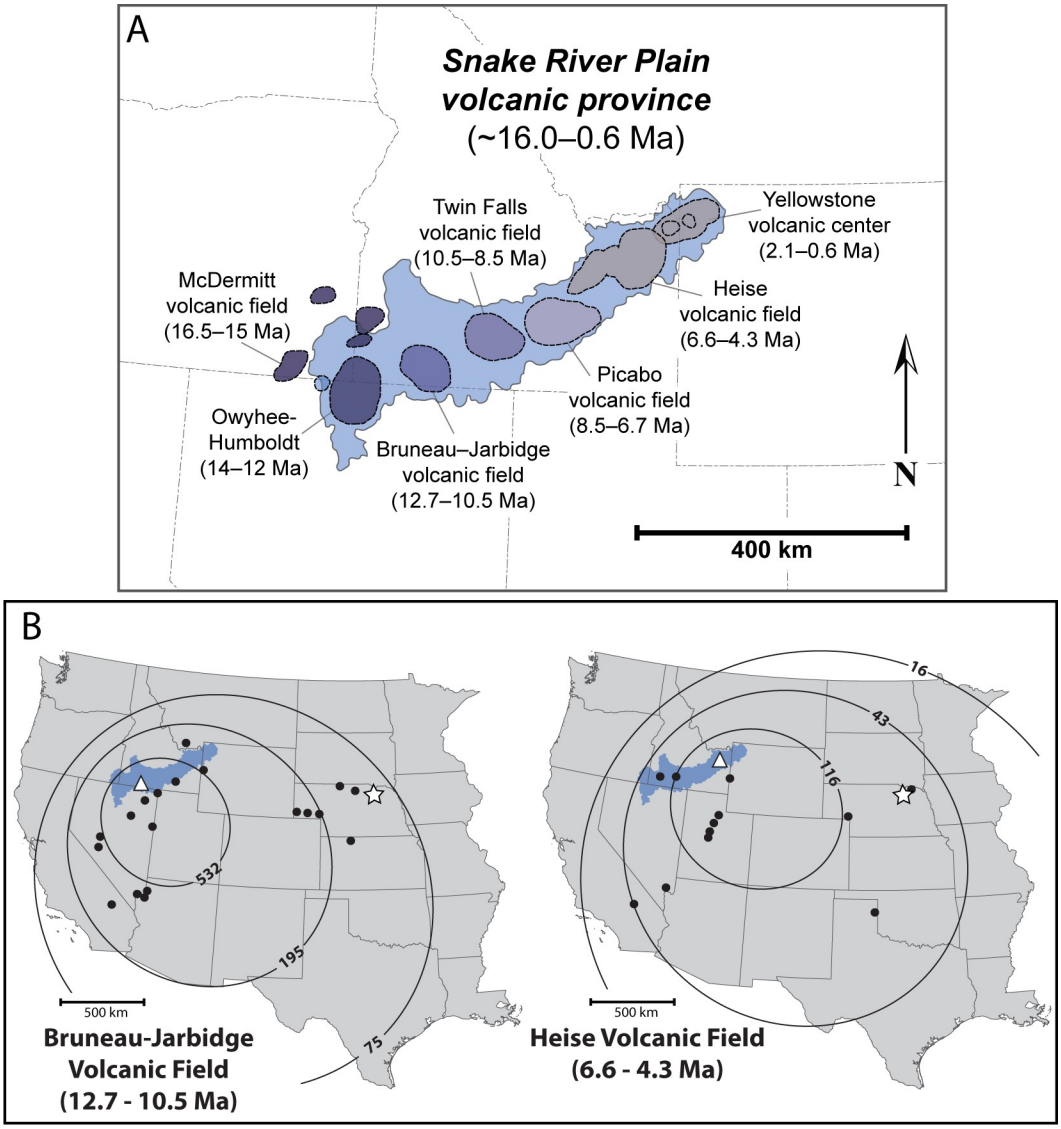

Fig 4. (A) The Snake River Plain Volcanic Province and its constituent volcanic fields and their age ranges of magmatic activity; modified from Perkins and Nash [16]. (B) Apparent accumulation rates (cm/m.y.) of ash beds from Bruneau-Jarbidge and Heise volcanic fields; modified from Perkins [43]. Note approximate locations of source calderas (white triangles), recognized airfall tuff deposits (black dots), and the Ashfall Fossil Beds and Grove Lake study area (white star). Base maps downloaded and modified from the USGS National Map Viewer (open access) at https://viewer.nationalmap.gov/viewer/.

https://doi.org/10.1371/journal.pone.0207103.g004

away prior to sample collection in order to maximize sample quality and avoid contamination with younger material washed down on the exposed face of the outcrop. At both locations, the first samples were taken from the bottom ~1–2 cm of the ash above the basal contact, which contained coarser-grained material and was darker gray than the overlying ash (Fig 3D). We moved up-section for the three remaining samples at each site, taking one sample approximately every 50–80 cm (Fig 5).

We isolated zircons from the ash samples using standard mineral separation techniques at the University of Kansas Isotope Geochemistry Laboratories (IGL). Each 1-liter sample was processed with an ultrasonic clay separator (UCS), using the methods described by Hoke et al.

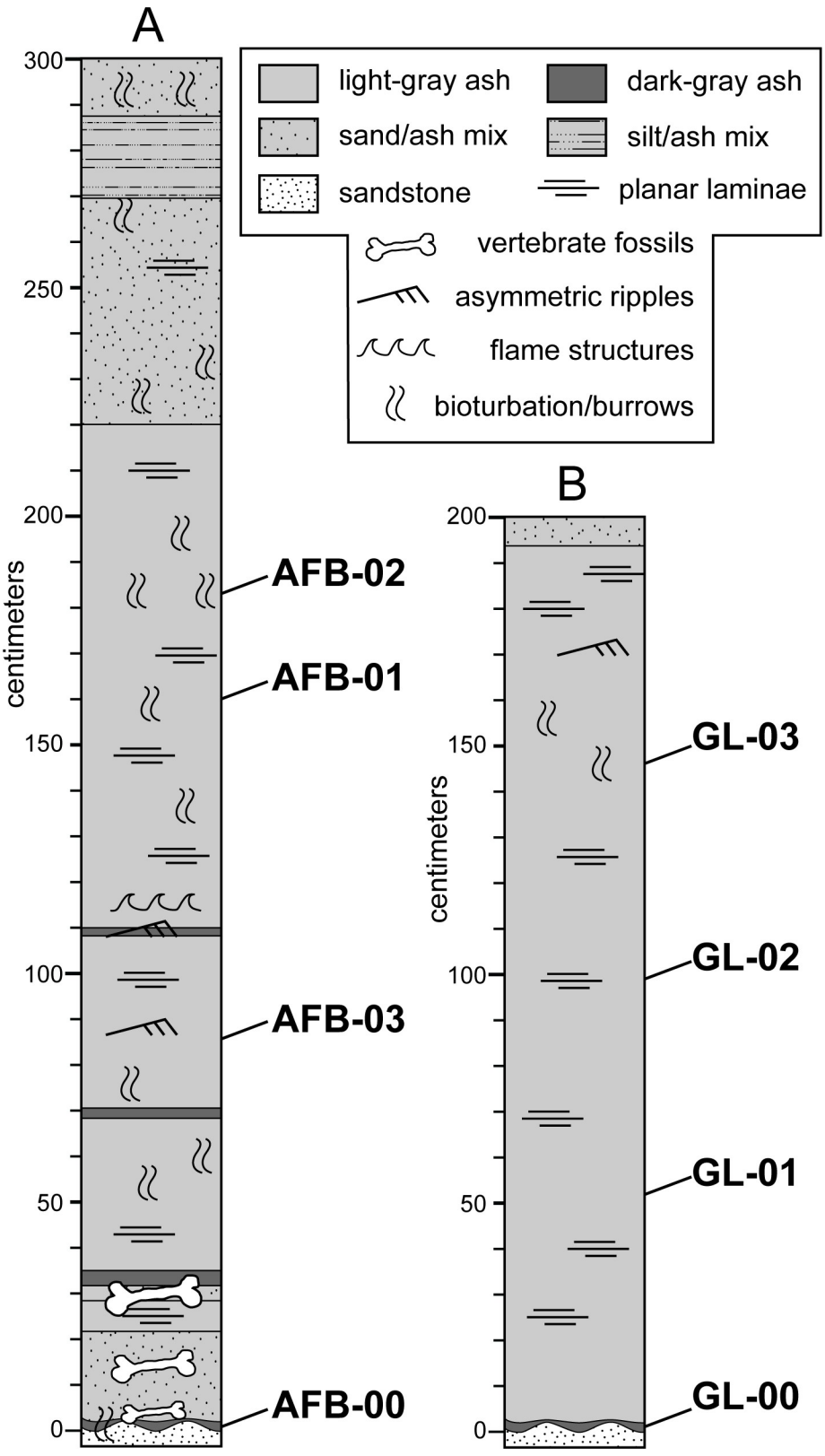

Fig 5. Measured sections of ash bed deposits in this study. (A) Ashfall Fossil Beds and (B) Grove Lake sections showing stratigraphic location of samples (AFB and GL, respectively). Some details of Ashfall Fossil Beds measured section (A) after Scheel and Rogers [10].

https://doi.org/10.1371/journal.pone.0207103.g005

[51], to separate high-density minerals. After drying, 150g of the high-density split of each sample was slowly added to a polytetrafluoroethylene (Teflon) container containing 12 N HF to dissolve the SiO_2-rich volcanic glass component of the ash. Finally, the remaining sample was again subjected to density separation, this time using heavy liquids (methylene iodide). Using a binocular microscope, zircon grains were handpicked from the high-density heavy liquid separates and mounted on double-sided adhesive tape on 1-inch diameter epoxy-resin discs. The grains were not polished to expose their interiors, in order to date the latest phase of zircon crystallization just prior to, or during, volcanic eruption [52].

Zircon U–Pb ages were obtained by laser ablation inductively coupled mass spectrometry (LA-ICP-MS) using a Thermo Scientific Element2 ICP-MS, attached to a Photon Machines Analyte.G2 193 nm ArF excimer laser ablation system. 20 μm circular spots were ablated with the laser at 2.0 J cm-2 fluence and 10 Hz repetition rate, resulting in pits of ~15 μm in depth from the surface towards the interior of each grain. Where feasible, the ablation targeted the tips of grains to avoid potentially older interiors an approach used in other studies (e.g. [53]). The ablated material was carried to the ICP-MS in He gas with a flow rate of 1.1 l/min, tied in with Ar gas of 1.1 l/min flow rate ca. 25 cm before entry into the plasma torch. Laser-induced fractionation, including elemental fractionation and downhole fractionation, and calibration drift were corrected by bracketing measurements of unknowns with the 608.5 ± 0.4 Ma GJ1 zircon reference material [54] and data reduction using the VizualAge data reduction scheme [55] for the IOLITE software package [56, 57]. Uncertainty (±2σ) in $^{206}Pb/^{238}U$ dates from individual GJ-1 ablations is approximately 8 Ma, uncertainties on larger data populations are at 1–2%. Calibration accuracy was monitored by measurement of zircon reference materials of known age during the same sessions, the Plešovice zircon [58] and Fish Canyon Tuff zircon [59], which were reproduced to within 1% of their published ages.

Our analytical results are presented using Isoplot 4.15 [60]. Kernel density estimates (KDEs) were produced using DensityPlotter 7.3 [61]. Eruption and maximum deposition ages (MDAs) of the volcanic ash deposits were derived from the youngest and most consistent grouping of concordant grains with overlapping U-Pb ages at 2σ. Because the Ashfall and Grove Lake samples contain large numbers of dates overlapping within 2 standard error (SE) uncertainties, we calculated the ages from analyses with a MSWD of 1 on the weighted average $^{206}Pb/^{238}U$ age (i.e. the scatter between analyses is equal to that expected for this number of analyses within a normal distribution). This is different from the approach to use the youngest three dates with overlapping uncertainties of Dickinson and Gehrels [62] proposed specifically for detrital populations that may contain only very few zircons close to the MDA. The rationale for our approach follows three main arguments. First, the measured dates represent zircon crystallization during the eruption event, or more likely, within the magma chamber before eruption. Crystallization within the magma chamber may have occurred over a time span longer than the uncertainty of the age determination, so including more analyses than expected from a normal distribution. Second, the calculated zircon age must be compared to Ar-Ar dates for these eruptions from the literature, which likely represent minimum (cooling) ages and are not influenced by "magma chamber inheritance". Including older zircons (MSWD >1) that may represent antecrystic zircon—crystals forming in the magma chamber significantly prior to the eruption (for a discussion of this term see e.g. [63, 64])—that will skew the calculated ages towards magma chamber process ages or even inherited earlier events. Third, extracting the age from only the youngest single analysis or very small group of analyses may bias the age determination towards a "tail" of the uncertainty distribution that is younger than the geological event and just represents statistical scatter. Hence the exclusion of a single concordant analysis from the interpretation of the Grove lake dataset. Analytical results are shown in S1 Table in Supporting Information.

Results

Ashfall Fossil Beds

At Ashfall Fossil Beds, two samples yielded zircons during mineral separation: AFB-00 and AFB-01 (Fig 5A). AFB-00 was collected from a ~2 cm-thick horizon at the base of the ash that is relatively coarse grained and darker gray than to the rest of the deposit (Fig 3D). AFB-01 was collected ~160 cm up section from the base were the deposit is light gray and a nearly pure vitric ash (Fig 3B). Only 5 zircon grains were recovered from AFB-01 and proved to be older, detrital grains that were therefore not used in the interpretation of the depositional age for the ash. AFB-00 yielded 136 zircon grains and the youngest concordant grouping of zircons with overlapping ages at 2σ is composed of 34 grains yielding a concordia age of 11.86 ± 0.13 Ma with a MSWD of 1.3 (Fig 6A and 6B). This is interpreted as a crystallization age and the maximum depositional age (MDA) of subsequent volcaniclastic deposition. A Kernel density plot

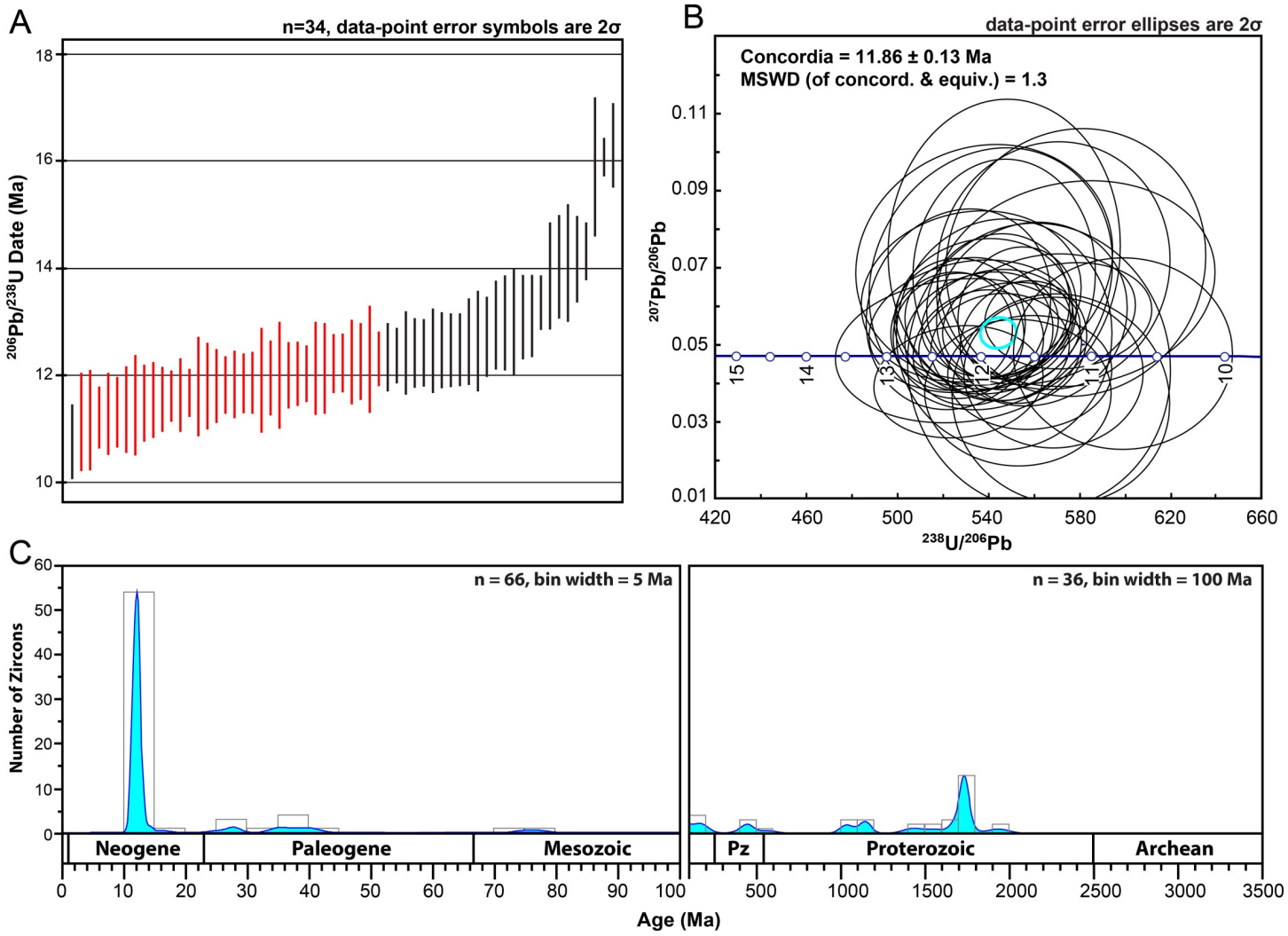

Fig 6. Zircon U-Pb results for the AFB-00 sample from Ashfall Fossil Beds. (A) U-Pb age ranges with 2σ error bars of the 61 youngest zircon grains plotted on a time axis showing 34 concordant analyses with an MSWD of ~1 (in red), used to calculate the MDA. (B) Tera-Wasserburg concordia diagram with MDA result of 11.86±0.13 Ma from 34 concordant analyses shown in 6A. (C) Kernel density estimate plot of AFB-00 showing $^{206}Pb/^{238}U$ (< 900 Ma) and $^{207}Pb/^{206}Pb$ (> 900 Ma) ages. MSWD = mean square weighted deviation; n = number of grains analyzed.

https://doi.org/10.1371/journal.pone.0207103.g006

of U-Pb ages from AFB-00 (Fig 6C) shows that while the largest and youngest age population is middle Miocene, there are smaller, yet significant, age populations dating back to ~1980 Ma; suggesting detrital input from extrabasinal detrital-source areas, rather than mineral fractions contributed by tephra.

Grove Lake

At Grove Lake, GL-00 was the only sample that yielded zircons during mineral separation (Fig 5B). As in AFB-00, sample GL-00 was collected from a ~2 cm-thick horizon at the base of the ash that is relatively coarse grained and darker gray than the rest of the overlying deposit (Fig 3C). In total, 102 grains from GL-00 were analyzed. Fifty-seven of the youngest concordant grains yield a weighted average $^{206}Pb/^{238}U$ age of 6.36 ± 0.06 with a MSWD of 1.0, and were used to calculate a concordia age of 6.42 ± 0.06 with a MSWD of 1.18 and interpreted as the crystallization age (Fig 7A and 7B). A Kernel density plot of U-Pb ages from GL-00 shows that

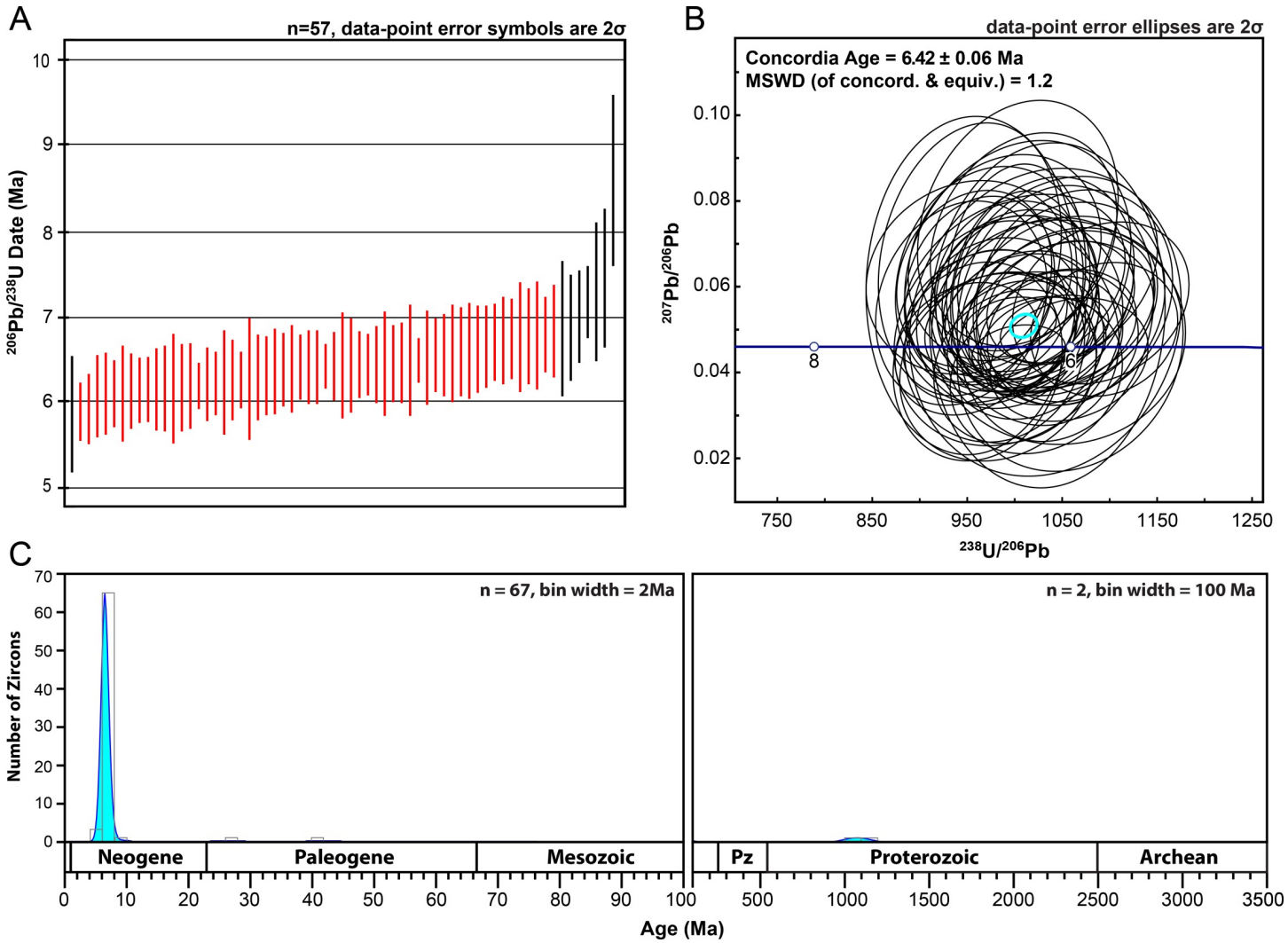

Fig 7. Zircon U-Pb results for the GL-00 sample from Grove Lake. (A) U-Pb ages ranges with 2σ error bars of the 65 youngest zircon grains plotted on a time axis showing 57 concordant analyses with an MSWD of 1 (in red), used to calculate the MDA. (B) Tera-Wasserburg concordia diagram with MDA result of 6.42±0.06 Ma from the 57 analyses with an MSWD of ~1 from 7A. (C) Kernel density plot of all GL-00 concordant results showing $^{206}Pb/^{238}U$ (< 900 Ma) and $^{207}Pb/^{206}Pb$ (> 900 Ma) ages. MSWD = mean square weighted deviation; n = number of grains analyzed.

https://doi.org/10.1371/journal.pone.0207103.g007

the largest age population is Late Miocene in age (Fig 7C). Smaller grain populations as old as ~1150 Ma suggest some detrital input, though less so than in the Ashfall Fossil beds deposit.

Discussion

Ash sources

The zircon U-Pb age of 11.86 ± 0.13 Ma for the Ashfall Fossil Beds ash sample (AFB-00) is too old to support correlation with the 10.45 ± 0.10 Ma age interpolated for the Cougar Point Tuff XV [15], as suggested by Dobbins [50] on the basis of major and trace element compositions. Our results do corroborate the age correlation of the Ashfall ash to supervolcanic eruptions originating from the Bruneau-Jarbidge caldera from ~12.7–10.5 Ma in southwestern Idaho (Fig 4) [16]. Specifically, the Ashfall U-Pb age chronologically overlaps with the $^{40}Ar/^{39}Ar$ ages of the Ibex Hollow and Cougar Point VII ignimbrites at Bruneau-Jarbidge (Fig 8).

The Ibex Hollow Tuff is an ~4 m thick, rhyolitic, nonwelded tuffs first described from the Trapper Creek area in south-central Idaho and initially referred to as the Tuff of Ibex Peak (tuff 30 in [65]). It was originally reported to have an $^{40}Ar/^{39}Ar$ age of 11.81 ± 0.03 Ma on sanidine (>0.5 mm), obtained by laser fusion [65]. After recalibration to the Fish Canyon Tuff standard, this age was later adjusted to 11.93 ± 0.03 Ma [15, 16]. The Cougar Point Tuff (CPT) VII is one of nine densely welded ignimbrites originating from the Bruneau-Jarbidge caldera that are best exposed in canyons along the Bruneau and Jarbidge rivers in southwestern Idaho [66]. Bonnichsen et al. [48] reported an $^{40}Ar/^{39}Ar$ age of 11.81 ± 0.03 Ma from sanidine phenocrysts. Perkins et al. [15] identified two additional ash fall tuffs from southwest Idaho that are within the AFB-00 age range; the Ibex Peak-8 (11.80 ± 0.04 Ma) and Logan Ranch ($^{40}Ar/^{39}Ar$ age of 11.79 ± 0.10 Ma) tuffs. Due to similarities in geochemical composition, stratigraphic position, and overlapping ages, however, Nash and Perkins [67] suspect that these ash beds are likely airfall equivalents of the CPT VII eruption event. Tephrochronologically correlated airfall equivalents of the Ibex Hollow and CPT VII tuffs are reported in multiple outcrops and cores from the Basin and Range province (Nevada and California), and the central Great Plains [16].

The U-Pb age of 6.42 ± 0.06 Ma for the Grove Lake ash (GL-00) coincides with supervolcanic activity in the Heise volcanic field (6.6–4.3 Ma) of the Snake River Plain in eastern Idaho (Fig 4). Our zircon-age is chronologically between, but does not overlap, with the $^{40}Ar/^{39}Ar$ ages of two well-documented ignimbrites of the Heise caldera; the Blacktail Creek and the Walcott tuffs (Fig 8). The Blacktail Creek Tuff is the most extensive ($>12^4$ km^2) welded ignimbrites of the Heise volcanic field [68] and has a mean $^{40}Ar/^{39}Ar$ age of 6.62 ± 0.03 Ma obtained from sanidine phenocrysts [69]. Morgan and McIntosh [69] geochemically correlate an airfall tuff with a younger $^{40}Ar/^{39}Ar$ age of 6.54 ± 0.06 Ma in the Palisades Reservoir area of Idaho. The smaller Walcott Tuff is a rhyolitic, welded ignimbrite that has a mean $^{40}Ar/^{39}Ar$ age of 6.27 ± 0.04 Ma also obtained from sanidine [69]. Blacktail Creek and Walcott tuffs have been tephrochronologically correlated to airfall ash beds in Idaho, Montana, Utah and the Great Plains region [16].

We consider our results as confirmation of the previously reported tephrochronologic correlations of the Ashfall Fossil Beds ash and Grove Lake ash to the Bruneau-Jarbidge and Heise volcanic fields, respectively. Correlating the Nebraskan ashes with specific $^{40}Ar/^{39}Ar$-dated Snake River Plain ignimbrites and airfall tuffs, however, is complicated by several factors. The $^{40}Ar/^{39}Ar$ ages of the various proximal ignimbrites near Bruneau-Jarbidge are statistically indistinguishable from our $^{206}Pb/^{238}U$ zircon crystallization ages at the 2σ level. In the case of the Grove Lake ash, our U-Pb age is outside the uncertainty ranges of Heise ignimbrites, though the Grove Lake age does overlap with $^{40}Ar/^{39}Ar$ ages of airfall tuffs near the Heise

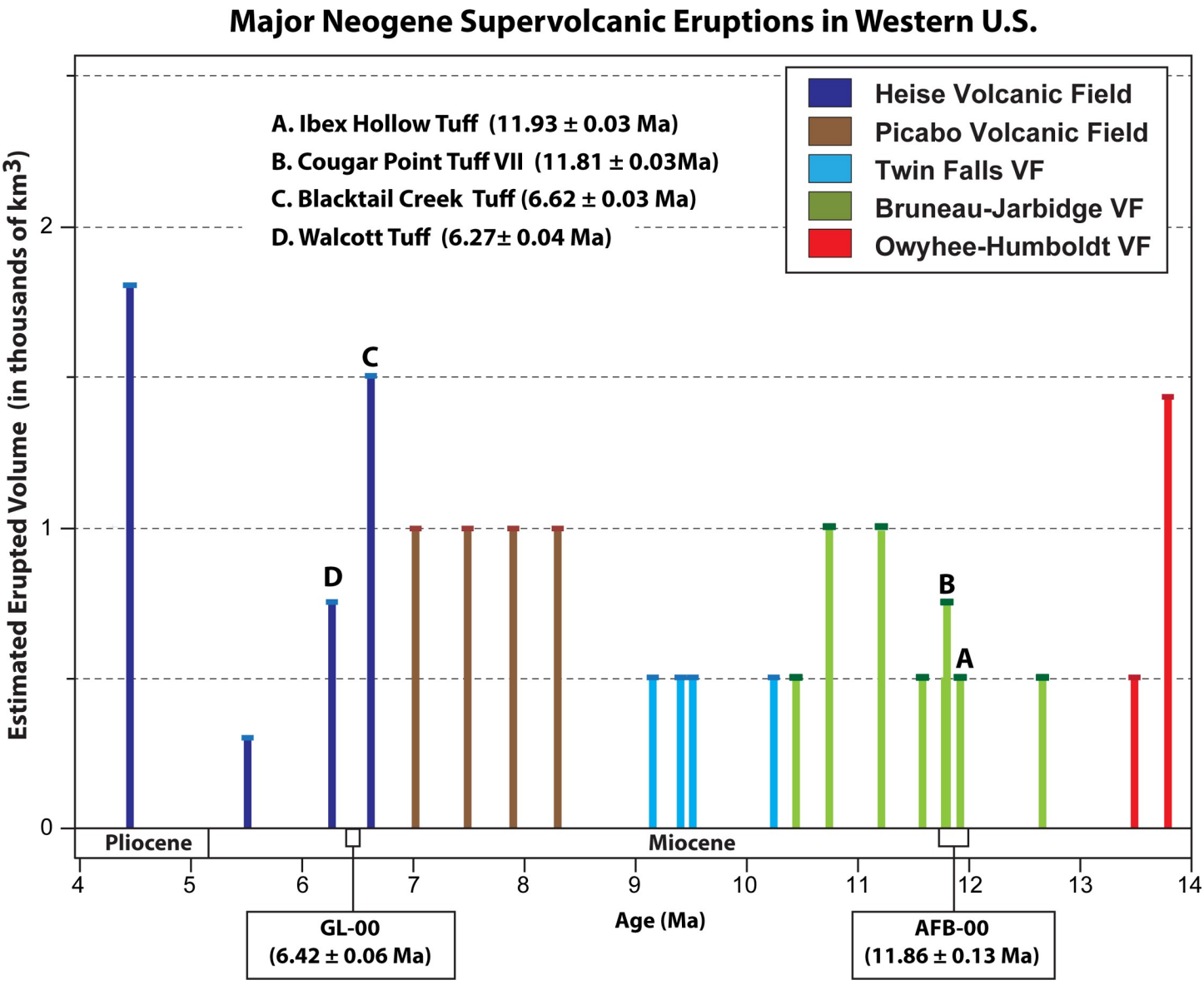

Fig 8. Ages and estimated volumes of known supervolcanic eruptions (ejecta volumes > 100 km^3) from the Snake River Plain hotspot and reportedly correlated with ash beds on the Great Plains. Eruption ages and ejecta volumes (estimated with large uncertainties; [49]) were derived from tuffs proximal to source calderas [15, 16, 48]. Colors indicate individual volcanic fields of origin, letters denote dated tuffs discussed in the text that fall within or are close in age with the U-Pb age ranges for sample AFB-00 and GL-00. See S2 Table in Supporting Information for the list of supervolcanic eruptions constituting this figure, modified and updated from Smith et al. [78].

https://doi.org/10.1371/journal.pone.0207103.g008

caldera [69]. Perceived age discrepancies could be the result of different crystallization histories of the different dated phenocrysts prior to or during the eruption phase and the lack of congruence between $^{206}Pb/^{238}U$ and $^{40}Ar/^{39}Ar$ geochronometers (see [70]). Geochronological studies on independently dated volcanic eruptions have shown that zircon crystallization ages may predate eruption by several thousands of years [e.g. 71]. Although it is beyond the scope of this paper, recent efforts inter-calibrate the U-Pb and $^{40}Ar/^{39}Ar$ dating series are reported for different systems in Sageman et al. [70], and Trujillo and Kowallis [72].

Implications of stratigraphic sampling of ash beds

Previous attempts to isolate zircons from the tephra at Ashfall were reportedly unsuccessful and it was assumed that radiogenic volcanoclastic material needed to date directly the *Konservat-Lagerstätte* was absent [2]. Given the lack of zircons throughout most of the 3 m-thick ash, it is evident that sampling from the ~1–2 cm horizon at the base of the ash was necessary in order to yield enough zircons for LA-ICP-MS analysis. If any previous sampling strategies overlooked this thin basal interval, it is indeed unlikely that such sampling would have yielded zircons indicative of the time of ash deposition. Rather, such hypothetical sampling would have yielded a low number of older detrital zircons, if any.

There are several *a priori* explanations for the concentration of zircons at the base of the ash bed, which include: 1) sorting during air transport, 2) heavier components of the ash cloud (e.g. zircons) precipitating to the ground before lighter components (e.g. glass, sanidine), and 3) internal stratification resulting from post-depositional reworking. Because of the lenticular morphology of the Ashfall ash (relatively thick in the immediate vicinity of the *Lagerstätte* and substantially thinner away from the *Lagerstätte*), it is interpreted to have infilled a paleodepression with ephemeral standing water [2]. Sedimentary structures such as asymmetrical ripples, planar laminae and flame structures suggest the presence of water in the paleodepression during ash accumulation. These structures in superposed ash intervals, as well as to multiple intervals of sediment bioturbation, suggest that the Ashfall ash bed is the product of a series of episodic depositional events likely separated by brief periods of subaerial exposure [10]. Furthermore, the presence of rounded, relatively old and large (up to ~100μm) detrital zircons indicates that the primary airfall deposit was mixed with sediment grains of other origins prior to final deposition at the site (Fig 6C). These pre-Neogene detrital zircons were likely derived from older deposits of the Ogallala Group. These lines of evidence indicate that the ash was reworked by water to some degree before infilling the topographic low at the Ashfall site.

Pyroclastic-fall deposits in submarine environments display a form of graded bedding characterized by an upward decrease in pyroclast density (e.g. [73, 74, 75, 76, 77]). If the ancient watering hole at all resembled a submarine environment in terms of depositional energy, this observation could explain the internal stratification seen in the Ashfall ash. The abundance of zircons in the lowest interval suggests that high density and/or coarser particles concentrated there via particle settling while the paleodepression was filled with a mixture of ash and water. Nevertheless, this pattern does not preclude sorting during air transport or prior, upwind precipitation of heavy minerals from the ash; these factors may also explain the observed upward decrease in density. In comparison, the ash bed at Grove Lake exhibits a similar style of internal stratification, but the dearth of information on the sedimentology of this ash hampers additional interpretation.

Conclusions

Studies using the direct radiometric dating and tephrochronology of airfall tephra constraint depositional ages of host strata and are vital for the development of a regional chronostratigraphic framework on the Great Plains. We report new U-Pb zircon ages for the Ashfall Fossil Beds and Grove Lake ashes of 11.86 ± 0.13 Ma and 6.42 ± 0.06, respectively. These analyses provide the first absolute age constraint for the Ashfall *Konservat-Lagerstätte* and are a direct test of reported, though not well- substantiated tephrochronologic studies correlating Ashfall with tephra of the Bruneau-Jarbidge volcanic field in the Snake River Plain Volcanic Province. However, age correlating the Ashfall and Grove Lake ashes with specific proximal ignimbrites and airfall tuffs for which $^{40}Ar/^{39}Ar$ ages are known is complicated by several factors. These factors include the range of uncertainty within the U-Pb results themselves, and the lack of

congruence between the $^{206}Pb/^{238}U$ and $^{40}Ar/^{39}Ar$ geochronometers. We plan to reduce the uncertainty and refine U-Pb zircon ages from Ashfall and Grove Lake using chemical abrasion isotope dilution thermal ionization mass spectrometry (CA-ID-TIMS), which uses dissolution of whole grains or parts of grains to obtain high-precision dates.

Our results also provide an admonition that applies to similar ash deposits of any age elsewhere. We opine that there should be no *a priori* expectation of uniform stratigraphic distribution of detrital and airfall zircons within ash bed deposits, particularly those showing evidence of being reworked. Only the lowermost ash layers in such a deposit can be expected to yield significant numbers of volcanic zircon. Thus, a closer examination of the distribution of zircons and other radiogenic mineral grains within airfall tephra deposits will likely determine the efficacy of different sampling strategies.

Supporting information

S1 Table. Zircon LA-ICP-MS U-Pb isotopic data used to calculate eruption ages for the Ashfall Fossil Beds (AFB-00) and Grove Lake (GL-00) ashbeds, Nebraska, USA.
(PDF)

S2 Table. Ages and estimated volumes of known supervolcanic eruptions (ejecta volumes > 100 km3) from the Snake River Plain hotspot and reportedly correlated with ash beds on the Great Plains.
(PDF)

Acknowledgments

This work is the result of a Senior Honors Thesis by Elijah Turner. Special thanks to Wayne Dickerson, Jeff Oalmann, Greg Ludvigson, Sandy Mosel (Ashfall Fossil Beds State Historical Park), Ken Terrell, and Mike Voorhies.

Author Contributions

Conceptualization: Jon J. Smith, R. M. Joeckel, Rick E. Otto.

Data curation: Andreas Möller.

Formal analysis: Jon J. Smith, Andreas Möller.

Funding acquisition: Jon J. Smith.

Investigation: Jon J. Smith, Elijah Turner, Andreas Möller.

Project administration: Jon J. Smith, Andreas Möller.

Resources: Andreas Möller, Rick E. Otto.

Supervision: Jon J. Smith.

Writing – original draft: Jon J. Smith, Elijah Turner.

Writing – review & editing: Jon J. Smith, Elijah Turner, Andreas Möller, R. M. Joeckel, Rick E. Otto.

References

1. Voorhies MR (1985) A Miocene rhinoceros herd buried in volcanic ash. National Geographic Society Research Reports 19: 671–688.

2. Tucker S, Otto R., Joeckel R., Voorhies M. (2014) The geology and paleontology of Ashfall Fossil Beds, a late Miocene (Clarendonian) mass-death assemblage, Antelope County and adjacent Knox County, Nebraska, USA. In: Korus JT, editor. Geologic Field Trips along the Boundary between the Central Lowlands and Great Plains. Geological Society of America Field Guide 36: 1–22.
3. Voorhies MR, Stover SG(1978) An articulated fossil skeleton of a pregnant rhinoceros Teleoceras major Hatcher. Proceedings of the Nebraska Academy of Sciences, 88th Annual Meeting, Lincoln, Nebraska, Abstracts: 48.
4. Voorhies MR, Thomasson JR (1979) Fossil grass anthoecia within Miocene rhinoceros skeletons: Diet in an extinct species. Science 206: 331–333. https://doi.org/10.1126/science.206.4416.331 PMID: 17733681
5. Voorhies MR (1990) Vertebrate biostratigraphy of the Ogallala Group in Nebraska. In: Gustavson TC, editor. Geologic Framework and Regional Hydrology: Upper Cenozoic Blackwater Draw and Ogallala Formations, Great Plains. Austin (TX), University of Texas, Bureau of Economic Geology: 115–151.
6. Voorhies MR (1992) Ashfall: Life and death at a Nebraska waterhole ten million years ago. University of Nebraska State Museum Notes 81: 1–4.
7. Beck DK (1995) Hypertrophic pulmonary osteodystrophy recognized in Teleoceras major (Mammalia: Rhinoceratidae) from the late Miocene of Nebraska. Geological Society of America Abstracts with Programs 27(3): 38.
8. Mead AJ (2000) Sexual dimorphism and paleoecology in Teleoceras, a North American Miocene rhinoceros. Paleobiology 26: 689–706.
9. Serieyssol CA, Slijk W, Edlund MB, Spaulding SA (2003) Miocene Diatoms from the Ashfall Fossil Beds near Royal, Nebraska. North American Diatom Symposium, 17th Meeting, Isla Morada, Miami, Florida, Abstracts: 37.
10. Scheel KE, Rogers RR (2010) A sedimentological analysis of an unconsolidated air-fall ash bed at Ashfall Fossil Beds, Nebraska. Geological Society of America Abstracts with Programs 42(5): 632.
11. Famoso NA, Pagnac D (2011) A Comparison of the Clarendonian Equid Assemblages from the Mission Pit, South Dakota and Ashfall Fossil Beds, Nebraska. Transactions of the Nebraska Academy of Sciences 32: 98–107.
12. Breining G (2007) Super Volcano: The Ticking Time Bomb Beneath Yellowstone National Park. 1st Edition. St. Paul: Voyageur Press. 256 p.
13. Bryan SE, Peate IU, Peate DW, Self S, Jerram DA, Mawby MR, et al. (2010) The largest volcanic eruptions on Earth. Earth-Science Reviews 102(3–4): 207–229.
14. Lowe DJ (2011) Tephrochronology and its application: a review. Quaternary Geochronology 6: 107–153.
15. Perkins ME, Brown FH, Nash WP, McIntosh W, Williams SK (1998) Sequence, age, and source of silicic fallout tuffs in middle to late Miocene basins of the northern Basin and Range province. Geological Society of America Bulletin 110: 344–360.
16. Perkins ME, Nash BP (2002) Explosive silicic volcanism of the Yellowstone hotspot: The ash fall tuff record. Geological Society of America Bulletin 114: 367–381.
17. Ludvigson GA, Sawin RS, Franseen EK, Watney WL, West RR, Smith JJ (2009) Review of the stratigraphy of the Ogallala Formation and revision of Neogene ("Tertiary") nomenclature in Kansas. Current Research in Earth Science, Kansas Geological Survey, Bulletin 256(2): 1–9.
18. Perkins ME, Diffendal R F Jr., Voorhies MR (1995a) Tephrochronology of the Ash Hollow Formation (Ogallala Group)-Northern Great Plains. Geological Society of America Abstracts with Programs 27(3): 79.
19. Perkins ME (1998a) Miocene ash beds and Miocene mammals in the intermontane west and Great Plains, USA. Journal of Vertebrate Paleontology 18(3): 70A.
20. Hedgecoe M (2000) Supervolcanoes [Series episode]. Horizon [TV Series], season 36, episode 13, BBC2, 3 Feb. 2000. Script available from http://www.bbc.co.uk/science/horizon/1999/ supervolcanoes_script.shtml.
21. Perkins ME, Diffendal RF Jr., Voorhies MR, Nash BP, Bailey BE (2014) Ashfall tephra in the Ogallala Group of the Great Plains: characteristics and significance. Geological Society of America Abstracts with Programs 46(4): 51.
22. Tedford RH, Albright LB III, Barnosky AD, Ferrusquia-Villafranca I, Hunt RM Jr., Storer JE, et al. (2004) Mammalian biochronology of the Arikareean through Hemphillian interval (late Oligocene through early Pliocene epochs). In: Woodburne MO, editor. Late Cretaceous and Cenozoic Mammals of North America, Geochronology and Biostratigraphy: New York, Columbia University Press: 167–231.
23. Voorhies MR (1981) Dwarfing the St. Helens Eruption: Ancient Ashfall Creates a Pompeii of Prehistoric Animals. National Geographic 159(1): 66–75.

24. Hochman G (1994) Buried in Ash [Series Episode]. Nova [TV Series], Season 21, episode 17, WGBH Educational Foundation, Boston (MA), 29 Nov. 1994. Synopsis available from http://www.worldcat.org/title/buried-in-ash/oclc/870178444.
25. Cook T (2017) Benchmarks–June 1977: First Excavations at Nebraska's Ashfall Fossil Beds. Earth Magazine of the American Geosciences Institute. May 2017 [cited April 2018]. Available from https://www.earthmagazine.org/article/benchmarks-june-1977-first-excavations-nebraskas-ashfall-fossil-beds
26. Schaltegger U, Schmitt AK, Horstwood MSA (2015) U–Th–Pb zircon geochronology by ID-TIMS, SIMS, and laser ablation ICP-MS: recipes, interpretations, and opportunities. Chemical Geology, 402: 89–110.
27. Skinner MF, Skinner SM, Gooris RJ (1968) Cenozoic rocks and faunas of Turtle Butte, south-central South Dakota. Bulletin of the American Museum of Natural History 138: 215–368.
28. Skinner MF, Johnson FW (1984) Tertiary stratigraphy and the Frick collection of fossil vertebrates from north-central Nebraska. Bulletin of the American Museum of Natural History 178: 215–368.
29. Diffendal RF Jr. (1982) Regional implications of the geology of the Ogallala Group (upper Tertiary) of southwestern Morrill County, Nebraska, and adjacent areas. Geological Society of America Bulletin 93: 964–976.
30. Gustavson TC, Winkler DA (1988) Depositional facies of the Miocene-Pliocene Ogallala Formation, northwestern Texas and eastern New Mexico. Geology 16(3): 203–206.
31. Diffendal RF Jr., Voorhies MR (1994) Geologic framework of the Niobrara River drainage basin and adjacent areas in South Dakota generally east of the 100th Meridian west longitude and west of the Missouri River. Nebraska Geological Survey Report of Investigations 9: 1–13.
32. Joeckel RM, Wooden SR Jr., Korus JT, Garbisch JO (2014) Architecture, heterogeneity, and origin of late Miocene fluvial deposits hosting the most important aquifer in the Great Plains, USA. Sedimentary Geology 311: 75–95.
33. Skinner MF, Taylor BE (1967) A revision of the geology and paleontology of the Bijou Hills, South Dakota. American Museum Novitates 2300: 1–53.
34. Skinner MF, Skinner SM, Gooris RJ (1977) Stratigraphy and biostratigraphy of late Cenozoic deposits in central Sioux County, western Nebraska. Bulletin of the American Museum of Natural History 158: 265–371.
35. Yatkola DA (1978) Tertiary Stratigraphy of the Niobrara River Valley, Marsland Quadrangle, Western Nebraska. Nebraska Geological Survey Paper 19: 1–66.
36. Holman JA (1971) Climatic significance of giant tortoises from the Wood Mountain Formation (upper Miocene) of Saskatchewan. Canadian Journal of Earth Sciences 8: 1148–1151.
37. Voorhies MR (1977) Giant tortoises—Fossil evidence of former subtropical climate on the Great Plains. University of Nebraska State Museum Notes 59: 1–4.
38. Caywood DD, Kramek BA, Feeney DA, Johnston GR (1985) Hypertrophic osteopathy associated with a bronchial foreign body and lobar pneumonia in a dog. Journal of the American Veterinary Medical Association 186: 698–700. PMID: 3988602
39. Leeman WP (1982) Development of the Snake River Plain-Yellowstone Plateau province, Idaho and Wyoming: an overview and petrologic model. In: Bonnichsen B, Breckenridge RM, editors. Cenozoic Geology of Idaho. Idaho Bureau of Mines and Geology Bulletin 26: p. 155–177.
40. Armstrong RL (1975) Precambrian (1500 m.y. old) rocks of central Idaho–the Salmon River Arch and its role in Cordilleran sedimentation and tectonics. American Journal of Science 275-A: 437–467.
41. Armstrong RL, Leeman WP, Malde HE (1975) K-Ar dating, Quaternary and Neogene volcanic rocks of the Snake River Plain, Idaho. American Journal of Science 264: 225–251.
42. Rose WI, Riley CM, Dartevelle S. (2003) Sizes and shapes of 10-Ma distal fall pyroclasts in the Ogallala Group, Nebraska. The Journal of Geology 111(1): 115–124.
43. Perkins ME (1998b) Tephrochronologic and volcanologic studies of silicic fallout tuffs in Miocene basins of the northern Basin and Range Province, U.S.A [Dissertation]. Salt Lake City (UT): The University of Utah, 206 p.
44. Slate JL, Sarna-Wojcicki AM, Wan E, Koning DJ, Connell SD, Dethier DP, et al. (2007) Upper Neogene tephrochronologic correlations in the northern Rio Grande Rift, New Mexico and southern Colorado. Geological Society of America Abstracts with Programs 39(6): 495.
45. Smith JJ, Layzell AL, Lukens W, Morgan ML, Keller SM, Martin RA, et al. (2016) Getting to the bottom of the High Plains aquifer: New insights into the depositional history, stratigraphy, and paleoecology of the Cenozoic High Plains. Geological Society of America Field Guides 44: 93–124.
46. Hallman JA(2016) Spatial and temporal patterns of Ogallala Formation deposition revealed by U-Pb zircon geochronology [M.Sc. Thesis]. Lawrence (KS): University of Kansas, 94 p.

47. Sitek BC (2017) Analyzing the Cenozoic Depositional History of Western Kansas: A New Approach Using Paleosol Zircon Geochronology [M.Sc. Thesis]. Lawrence (KS): University of Kansas, 49 p.
48. Bonnichsen B, Leeman WP, Honjo N, McIntosh WC, Godchaux MM (2008) Miocene silicic volcanism in southwestern Idaho: Geochronology, geochemistry, and evolution of the central Snake River Plain. Bulletin of Volcanology 70: 315–342, https://doi.org/10.1007/s00445-007-0141-6
49. Mason BG, Pyle DM, Oppenheimer C (2004) The size and frequency of the largest explosive eruptions on Earth. Bulletin of Volcanology 66: 735–748.
50. Dobbins J (2010) A Geochemical Analysis of the Tuffaceous Deposit at Ashfall Fossil Beds, Nebraska [Senior Honors Thesis]. St Paul (MN): Macalester College, 44 p.
51. Hoke GD, Schmitz MD, Bowring SA (2014) An ultrasonic method for isolating nonclay components from clay-rich material. Geochemistry, Geophysics, Geosystems 15: 492–498.
52. Reid MR, Coath CD (2000) In situ U–Pb ages of zircons from the Bishop Tuff; no evidence for long crystal residence times. Geology 28: 443–446.
53. Rubin A, Cooper KM, Leever M, Wimpenny J, Deering C, Rooney T, et al. (2016) Changes in magma storage conditions following caldera collapse at Okataina Volcanic Center, New Zealand. Contributions to Mineralogy and Petrology 171: 1–18.
54. Jackson SE, Pearson NJ, Griffin WL, Belousova EA (2004) The application of laser ablation-inductively coupled plasma-mass spectrometry to in situ U–Pb zircon geochronology. Chemical Geology 211: 47–69.
55. Petrus JA, Kamber BS (2012) VizualAge: A novel approach to laser ablation ICP-MS U-Pb geochronology data reduction. Geostandards and Geoanalytical Research 36: 247–270.
56. Paton C, Woodhead JD, Hellstrom JC, Hergt JM, Greig A, Maas R (2010) Improved laser ablation U-Pb geochronology through robust downhole fractionation correction. Geochemistry, Geophysics, Geosystems 11: 36 p.
57. Paton C, Hellstrom J, Paul B, Woodhead J, Hergt J (2011) Iolite: Freeware for the visualization and processing of mass spectrometric data. Journal of Analytical Atomic Spectrometry 26: 2508–2518.
58. Sláma J, Košler J, Condon DJ, Crowley JL, Gerdes A, Hanchar JM, et al. (2008) Plešovice zircon–A new natural reference material for U-Pb and Hf isotopic microanalysis. Chemical Geology 249: 1–35.
59. Wotzlaw JF, Schaltegger U, Frick DA, Dungan MA, Gerdes A, Günther D (2013) Tracking the evolution of large-volume silicic magma reservoirs from assembly to supereruption. Geology 41: 867–70.
60. Ludwig KR (2012) Isoplot 4.15: a geochronological toolkit for Microsoft Excel. Berkeley Geochronology Center Special Publication 5, revised January 30, 2012.
61. Vermeesch P (2012) On the visualisation of detrital age distributions. Chemical Geology 312–313: 190–194.
62. Dickinson WR, Gehrels GE (2009) Use of U-Pb ages of detrital zircons to infer maximum depositional ages of strata: a test against a Colorado Plateau Mesozoic database. Earth and Planetary Science Letters 288: 115–125.
63. Bacon CR, Lowenstern JB (2005) Late Pleistocene granodiorite source for recycled zircon and phenocrysts in rhyodacite lava at Crater Lake, Oregon. Earth Planetary Science Letters 233: 277–293.
64. Schoene B, Schaltegger U, Brack P, Latkoczy C, Stracke A, Günther D. (2012) Rates of magma differentiation and emplacement in a ballooning pluton recorded by U–Pb TIMS-TEA, Adamello batholith, Italy. Earth and Planetary Science Letters 355–356: 162–173.
65. Perkins ME, Nash WP, Brown FH, Fleck RJ (1995b) Fallout tuffs of Trapper Creek Idaho—A record of Miocene explosive volcanism in the Snake River Plain volcanic province. Geological Society of America Bulletin 107: 1484–1506.
66. Bonnichsen B, Citron GP (1982) Cougar Point Tuff, southwestern Idaho and vicinity, In: Bonnichsen B, Breckenridge RM, eds. Cenozoic Geology of Idaho. Idaho Bureau of Mines and Geology Bulletin 26: 255–281.
67. Nash BP, Perkins ME (2012) Neogene Fallout Tuffs from the Yellowstone Hotspot in the Columbia Plateau Region, Oregon, Washington and Idaho, USA. PLoS ONE 7(10):e44205. https://doi.org/10.1371/journal.pone.0044205 PMID: 23071494
68. Morgan LA, Doherty DJ, Leeman WP (1984) Ignimbrites of the eastern Snake River Plain, Idaho: Evidence for major caldera-forming eruptions. Journal of Geophysical Research 89: 8665–8678.
69. Morgan LA, McIntosh WC (2005) Timing and development of the Heise volcanic field, Snake River Plain, Idaho, western USA. GSA Bulletin 117(3/4): 288–306.
70. Sageman BB, Singer BS, Meyers SR, Siewert SE, Walaszczyk I, Condon DJ, et al. (2014) Integrating 40Ar/39Ar, U-Pb, and astronomical clocks in the Cretaceous Niobrara Formation, Western Interior Basin, USA. GSA Bulletin 126(7–8): 956–973.

71. Storm S, Shane P, Schmitt AK, Lindsay JM (2011) Contrasting punctuated zircon growth in two syn-erupted rhyolite magmas from Tarawera volcano: Insights to crystal diversity in magmatic systems. Earth and Planetary Science Letters 301: 511–20.

72. Trujillo KC, Kowallis BJ (2015) Recalibrated legacy $^{40}Ar/^{39}Ar$ ages for the Upper Jurassic Morrison Formation, Western Interior, U.S.A. Geology of the Intermountain West 2: 1–8.

73. Fiske RS (1963) Subaqueous pyroclastic flows in the Ohanapecosh Formation, Washington. Geological Society of America Bulletin 74: 391–406.

74. Fiske RS, Matsuda T (1964) Submarine equivalents of ash flows in the Tokiwa Formation, Japan. American Journal of Science 262: 76–106.

75. Fiske RS (1964) Vertical grading of fragment density in subaqueous pyroclastic flows. Geological Society of America Special Paper 76: 59.

76. Fiske RS (1969) Recognition and significance of pumice in marine pyroclastic rocks. Geological Society of America Bulletin 80: 1–8.

77. Niem AR (1977) Mississippian pyroclastic flow and ash-fall deposits in the deep-marine Ouachita flysch basin, Oklahoma and Arkansas. Geological Society of America Bulletin 88: 49–61.

78. Smith JJ, Ludvigson GA, Layzell A, Möller A, Harlow RH, Turner E, et al. (2017) Discovery of Paleogene deposits of the central High Plains aquifer in the western Great Plains, USA. Journal of Sedimentary Research 87: 880–896, https://doi.org/10.2110/jsr.2017.48.

S1 Table. Zircon LA-ICP-MS U-Pb Isotopic Data and Ages for Smith et al., First U-Pb Zircon Ages from Ashfall Fossil Beds (AFB-00) and Grove Lake (GL-00), Nebraska, USA

						Corrected Isotopic Ratios							Ages (Ma)[h]							
Sample ID	Grain #[a]	U[b] [ppm]	Th[b] [ppm]	Th/U	eU[c] [ppm]	$^{207}Pb/^{235}U$[d]	±2s[e]	$^{206}Pb/^{238}U$[d]	±2s[e]	Rho[f]	$^{207}Pb/^{206}Pb$[g]	±2s[e]	$^{207}Pb/^{235}U$	±2s	$^{206}Pb/^{238}U$	±2s	$^{207}Pb/^{206}Pb$	±2s	Disc. %[k]	Wtd. Disc.[l]
AFB-00	AFB_49	106.3	60.5	0.57	120.52	0.01	0.005	0.0017	0.0001	-0.24	0.057	0.024	11.9	5.0	10.8	0.7	40.0	690.0	-10.6	0.2
AFB-00	AFB_112	48.9	27.4	0.56	55.33	0.02	0.010	0.0017	0.0002	-0.11	0.107	0.050	18.2	9.9	10.9	1.0	-500.0	1000.0	-67.0	0.7
AFB-00	AFB_140	166.5	91.0	0.55	187.89	0.02	0.005	0.0017	0.0001	0.18	0.074	0.018	18.7	4.4	11.1	0.5	710.0	470.0	-68.5	1.7
AFB-00	AFB_133	94.8	40.8	0.43	104.39	0.02	0.007	0.0017	0.0001	-0.10	0.075	0.034	16.7	6.8	11.1	0.9	240.0	730.0	-50.0	0.8
AFB-00	AFB_77	125.7	65.0	0.52	140.98	0.02	0.005	0.0017	0.0002	-0.20	0.072	0.025	15.6	5.2	11.2	0.9	270.0	630.0	-39.8	0.9
AFB-00	AFB_42	156.3	107.3	0.69	181.52	0.01	0.003	0.0017	0.0001	-0.16	0.058	0.013	13.7	2.7	11.2	0.6	280.0	360.0	-22.2	0.9
AFB-00	AFB_128	98.6	60.1	0.61	112.72	0.01	0.005	0.0018	0.0001	-0.15	0.050	0.028	9.1	5.3	11.3	0.8	-540.0	680.0	19.3	-0.4
AFB-00	AFB_129	126.2	89.8	0.71	147.30	0.01	0.004	0.0018	0.0001	-0.10	0.045	0.018	10.3	3.9	11.3	0.7	-180.0	510.0	8.9	-0.3
AFB-00	AFB_105	103.3	61.2	0.59	117.68	0.02	0.006	0.0018	0.0001	0.00	0.070	0.028	16.8	6.4	11.4	0.8	350.0	700.0	-47.9	0.9
AFB-00	AFB_73	160.2	98.2	0.61	183.28	0.02	0.003	0.0018	0.0001	0.18	0.068	0.015	16.5	3.4	11.4	0.7	510.0	410.0	-44.4	1.5
AFB-00	AFB_99	76.6	36.2	0.47	85.11	0.01	0.008	0.0018	0.0002	-0.09	0.038	0.030	10.5	7.5	11.4	0.9	-290.0	720.0	8.2	-0.1
AFB-00	AFB_94	191.2	116.8	0.61	218.65	0.02	0.005	0.0018	0.0001	-0.03	0.107	0.023	24.2	5.0	11.5	0.7	1470.0	460.0	-111.4	2.6
AFB-00	AFB_143	226.7	134.6	0.59	258.33	0.01	0.003	0.0018	0.0001	0.04	0.059	0.014	13.9	3.3	11.5	0.7	270.0	410.0	-21.1	0.7
AFB-00	AFB_30	121.6	69.0	0.57	137.82	0.01	0.005	0.0018	0.0001	0.11	0.057	0.020	14.2	4.8	11.5	0.7	350.0	540.0	-23.1	0.6
AFB-00	AFB_127	142.1	73.7	0.52	159.42	0.01	0.003	0.0018	0.0001	-0.13	0.043	0.012	10.6	3.0	11.6	0.6	-240.0	400.0	8.2	-0.3
AFB-00	AFB_102	154.1	93.3	0.61	176.03	0.02	0.004	0.0018	0.0001	-0.02	0.081	0.017	20.9	4.1	11.6	0.6	960.0	410.0	-80.6	2.3
AFB-00	AFB_27	155.9	92.9	0.60	177.73	0.01	0.003	0.0018	0.0001	0.07	0.050	0.013	12.5	3.3	11.6	0.5	20.0	420.0	-7.7	0.3
AFB-00	AFB_114	114.4	68.7	0.60	130.54	0.01	0.004	0.0018	0.0001	-0.08	0.041	0.017	9.2	3.9	11.6	0.7	-370.0	480.0	20.9	-0.6
AFB-00	AFB_144	177.5	126.7	0.71	207.27	0.01	0.004	0.0018	0.0001	0.06	0.059	0.015	14.4	3.5	11.7	0.5	190.0	420.0	-23.4	0.8
AFB-00	AFB_139	213.0	157.0	0.74	249.90	0.02	0.008	0.0018	0.0001	-0.02	0.108	0.080	18.6	8.0	11.8	0.9	800.0	940.0	-57.8	0.9
AFB-00	AFB_55	91.4	39.8	0.44	100.75	0.01	0.006	0.0018	0.0001	0.14	0.056	0.028	13.0	6.2	11.8	0.8	-400.0	640.0	-10.2	0.2
AFB-00	AFB_56	129.7	73.3	0.57	146.93	0.02	0.006	0.0018	0.0001	-0.02	0.084	0.024	21.8	5.8	11.8	0.7	1030.0	530.0	-84.7	1.7
AFB-00	AFB_122	103.9	49.9	0.48	115.63	0.02	0.006	0.0018	0.0001	-0.35	0.075	0.028	17.0	6.2	11.8	0.7	80.0	660.0	-44.1	0.8
AFB-00	AFB_93	164.8	101.6	0.62	188.68	0.01	0.003	0.0018	0.0001	-0.10	0.053	0.012	12.4	2.9	11.8	0.5	330.0	370.0	-4.9	0.2
AFB-00	AFB_98	183.8	120.9	0.66	212.21	0.02	0.004	0.0018	0.0001	0.03	0.087	0.015	21.3	3.5	11.8	0.6	1070.0	340.0	-80.2	2.7
AFB-00	AFB_84	167.0	114.4	0.69	193.88	0.01	0.003	0.0018	0.0001	0.01	0.053	0.013	13.0	2.9	11.8	0.6	190.0	380.0	-9.9	0.4
AFB-00	AFB_67	158.0	99.6	0.63	181.41	0.02	0.004	0.0018	0.0001	0.12	0.067	0.016	15.1	3.9	11.9	0.6	390.0	440.0	-27.4	0.8
AFB-00	AFB_52	177.2	127.0	0.72	207.05	0.01	0.003	0.0018	0.0001	0.14	0.055	0.011	14.0	2.9	11.9	0.6	240.0	360.0	-18.0	0.7
AFB-00	AFB_8	87.4	67.2	0.77	103.19	0.02	0.007	0.0018	0.0002	-0.16	0.102	0.035	21.6	6.7	11.9	1.3	730.0	670.0	-81.5	1.4
AFB-00	AFB_80	91.0	47.7	0.52	102.21	0.02	0.007	0.0019	0.0002	0.07	0.074	0.031	16.7	6.9	11.9	1.0	-30.0	760.0	-40.2	0.7
AFB-00	AFB_92	141.7	79.8	0.56	160.45	0.01	0.004	0.0019	0.0001	-0.14	0.065	0.019	14.9	4.0	12.0	0.7	260.0	500.0	-24.7	0.7
AFB-00	AFB_14	104.1	65.9	0.63	119.59	0.02	0.006	0.0019	0.0002	-0.12	0.069	0.030	18.1	6.4	12.0	1.0	200.0	700.0	-50.8	1.0
AFB-00	AFB_104	175.2	111.3	0.64	201.36	0.01	0.003	0.0019	0.0001	0.04	0.052	0.012	13.6	3.2	12.0	0.6	-30.0	380.0	-13.3	0.5
AFB-00	AFB_32	150.0	79.9	0.53	168.78	0.01	0.004	0.0019	0.0001	0.27	0.058	0.014	14.6	3.8	12.0	0.6	120.0	420.0	-21.4	0.7
AFB-00	AFB_37	181.1	130.6	0.72	211.79	0.01	0.003	0.0019	0.0001	0.02	0.049	0.012	12.6	3.1	12.0	0.5	-10.0	390.0	-4.7	0.2
AFB-00	AFB_86	164.0	110.2	0.67	189.90	0.02	0.003	0.0019	0.0001	0.10	0.078	0.014	19.5	3.2	12.1	0.6	910.0	350.0	-61.4	2.3
AFB-00	AFB_70	201.0	136.0	0.68	232.96	0.02	0.005	0.0019	0.0001	-0.03	0.071	0.026	16.1	4.7	12.1	0.9	480.0	530.0	-32.7	0.8
AFB-00	AFB_107	161.0	96.1	0.60	183.58	0.01	0.004	0.0019	0.0001	0.11	0.057	0.017	14.1	3.6	12.1	0.9	110.0	470.0	-16.2	0.5
AFB-00	AFB_88	820.0	501.0	0.61	937.74	0.03	0.004	0.0019	0.0001	0.46	0.094	0.013	25.1	3.2	12.2	0.7	1430.0	260.0	-105.9	4.0
AFB-00	AFB_57	188.9	116.1	0.61	216.18	0.01	0.004	0.0019	0.0001	0.19	0.060	0.014	14.5	3.6	12.2	0.6	350.0	410.0	-18.7	0.6
AFB-00	AFB_53	171.3	103.9	0.61	195.72	0.01	0.004	0.0019	0.0001	-0.03	0.058	0.014	13.6	3.5	12.2	0.6	270.0	390.0	-11.2	0.4
AFB-00	AFB_111	89.4	37.9	0.42	98.31	0.02	0.006	0.0019	0.0001	0.05	0.060	0.022	15.3	5.5	12.3	0.8	100.0	560.0	-24.9	0.6
AFB-00	AFB_28	131.2	70.9	0.54	147.86	0.01	0.003	0.0019	0.0001	0.10	0.039	0.012	10.5	3.1	12.3	0.7	-160.0	400.0	14.4	-0.6
AFB-00	AFB_147	114.3	69.1	0.60	130.54	0.01	0.004	0.0019	0.0002	-0.02	0.051	0.017	12.6	4.0	12.3	1.0	350.0	490.0	-2.4	0.1
AFB-00	AFB_76	179.0	119.0	0.66	206.97	0.01	0.003	0.0019	0.0001	0.12	0.055	0.013	14.1	3.3	12.3	0.5	480.0	370.0	-14.5	0.5
AFB-00	AFB_71	155.8	94.5	0.61	178.01	0.02	0.005	0.0019	0.0001	0.19	0.062	0.020	16.7	5.0	12.3	0.6	380.0	540.0	-35.3	0.9
AFB-00	AFB_110	240.1	216.8	0.90	291.05	0.01	0.002	0.0019	0.0001	0.21	0.049	0.008	12.0	1.9	12.4	0.5	120.0	280.0	3.0	-0.2
AFB-00	AFB_17	90.6	54.8	0.60	103.48	0.01	0.005	0.0019	0.0001	0.06	0.053	0.019	14.0	4.7	12.4	0.8	-40.0	510.0	-12.7	0.3
AFB-00	AFB_108	134.2	92.7	0.69	155.98	0.01	0.003	0.0019	0.0001	0.07	0.057	0.014	13.8	3.4	12.4	0.7	250.0	420.0	-11.1	0.4
AFB-00	AFB_142	242.0	159.5	0.66	279.48	0.01	0.003	0.0019	0.0001	0.07	0.059	0.012	14.7	3.0	12.4	0.6	460.0	350.0	-18.4	0.8
AFB-00	AFB_6	114.0	73.1	0.64	131.18	0.03	0.006	0.0019	0.0001	0.16	0.101	0.023	24.8	5.5	12.4	0.7	1140.0	440.0	-99.4	2.2
AFB-00	AFB_85	107.0	55.0	0.51	119.93	0.01	0.005	0.0019	0.0001	0.02	0.048	0.021	9.2	5.1	12.5	0.8	-180.0	590.0	26.2	-0.6
AFB-00	AFB_12	119.5	76.2	0.64	137.41	0.01	0.004	0.0019	0.0001	-0.32	0.058	0.017	13.7	4.1	12.5	0.7	130.0	470.0	-9.9	0.3

S1 Table. Zircon LA-ICP-MS U-Pb Isotopic Data and Ages for Smith et al., First U-Pb Zircon Ages from Ashfall Fossil Beds (AFB-00) and Grove Lake (GL-00), Nebraska, USA

						Corrected Isotopic Ratios							Ages (Ma)[h]							
Sample ID	Grain #[a]	U[b] [ppm]	Th[b] [ppm]	Th/U	eU[c] [ppm]	$^{207}Pb/^{235}U$[d]	±2s[e]	$^{206}Pb/^{238}U$[d]	±2s[e]	Rho[f]	$^{207}Pb/^{206}Pb$[g]	±2s[e]	$^{207}Pb/^{235}U$	±2s	$^{206}Pb/^{238}U$	±2s	$^{207}Pb/^{206}Pb$	±2s	Disc. %[k]	Wtd. Disc.[l]
AFB-00	AFB_148	112.0	63.2	0.56	126.85	0.01	0.005	0.0019	0.0001	-0.13	0.061	0.022	12.8	5.0	12.5	0.7	-50.0	520.0	-2.6	0.1
AFB-00	AFB_82	135.1	59.3	0.44	149.04	0.02	0.005	0.0019	0.0001	0.25	0.064	0.021	15.8	4.8	12.5	0.7	110.0	540.0	-26.6	0.7
AFB-00	AFB_5	98.1	49.5	0.50	109.73	0.04	0.008	0.0020	0.0001	0.45	0.145	0.031	34.4	8.0	12.6	0.8	1600.0	490.0	-172.6	2.7
AFB-00	AFB_43	69.1	35.5	0.51	77.44	0.02	0.008	0.0020	0.0001	0.17	0.065	0.031	18.2	7.9	12.6	0.8	-370.0	770.0	-44.1	0.7
AFB-00	AFB_123	93.3	55.8	0.60	106.41	0.01	0.006	0.0020	0.0002	-0.11	0.042	0.024	11.1	5.8	12.6	0.9	-480.0	660.0	12.2	-0.3
AFB-00	AFB_101	150.3	67.8	0.45	166.23	0.02	0.004	0.0020	0.0001	0.01	0.059	0.016	15.9	4.2	12.7	0.8	400.0	450.0	-25.0	0.8
AFB-00	AFB_33	51.7	39.5	0.76	60.98	0.08	0.015	0.0020	0.0002	0.41	0.304	0.056	80.0	13.0	12.8	1.4	3280.0	410.0	-525.0	5.2
AFB-00	AFB_1	114.2	69.8	0.61	130.60	0.04	0.005	0.0020	0.0001	-0.21	0.140	0.025	36.0	5.2	12.9	0.7	2030.0	320.0	-179.7	4.4
AFB-00	AFB_134	112.0	57.9	0.52	125.61	0.02	0.006	0.0020	0.0001	0.37	0.068	0.022	18.2	5.5	12.9	0.8	470.0	550.0	-40.6	1.0
AFB-00	AFB_62	121.5	78.6	0.65	139.97	0.02	0.007	0.0020	0.0001	0.04	0.053	0.022	15.3	6.8	13.0	0.9	100.0	630.0	-17.9	0.3
AFB-00	AFB_150	79.3	37.1	0.47	88.02	0.02	0.011	0.0020	0.0002	-0.20	0.093	0.043	23.0	11.0	13.0	1.0	880.0	870.0	-76.9	0.9
AFB-00	AFB_44	95.4	52.0	0.55	107.62	0.02	0.006	0.0020	0.0001	0.04	0.064	0.026	15.5	5.5	13.1	0.8	150.0	550.0	-18.4	0.4
AFB-00	AFB_130	124.0	71.5	0.58	140.80	0.02	0.005	0.0020	0.0001	0.06	0.066	0.021	15.2	5.0	13.1	0.8	-20.0	490.0	-15.9	0.4
AFB-00	AFB_60	166.0	90.9	0.55	187.36	0.03	0.005	0.0020	0.0001	0.23	0.093	0.018	25.2	4.8	13.1	0.8	1030.0	420.0	-91.9	2.5
AFB-00	AFB_46	101.3	53.0	0.52	113.76	0.04	0.007	0.0021	0.0001	0.29	0.155	0.025	38.5	6.4	13.3	0.8	2090.0	340.0	-190.1	3.9
AFB-00	AFB_78	761.0	143.5	0.19	794.72	0.01	0.001	0.0021	0.0001	-0.12	0.052	0.006	14.3	1.3	13.4	0.5	180.0	180.0	-7.0	0.7
AFB-00	AFB_63	137.8	65.6	0.48	153.22	0.05	0.009	0.0022	0.0002	0.55	0.153	0.031	44.3	9.0	13.9	1.0	2220.0	390.0	-219.6	3.4
AFB-00	AFB_69	94.2	40.6	0.43	103.74	0.05	0.007	0.0022	0.0002	0.06	0.191	0.028	53.1	7.3	14.0	1.0	2610.0	260.0	-278.5	5.4
AFB-00	AFB_103	157.0	101.7	0.65	180.90	0.06	0.015	0.0022	0.0002	0.40	0.199	0.049	56.0	15.0	14.1	1.1	2300.0	590.0	-297.2	2.8
AFB-00	AFB_74	148.7	95.2	0.64	171.07	0.02	0.007	0.0022	0.0001	0.21	0.074	0.025	18.6	6.7	14.2	0.8	440.0	570.0	-31.3	0.7
AFB-00	AFB_141	205.0	102.0	0.50	228.97	0.03	0.005	0.0022	0.0001	0.27	0.094	0.013	30.3	4.4	14.3	0.5	1480.0	280.0	-111.6	3.6
AFB-00	AFB_68	120.6	60.5	0.50	134.82	0.09	0.026	0.0025	0.0002	0.24	0.240	0.051	82.0	20.0	15.9	1.3	2520.0	460.0	-415.7	3.3
AFB-00	AFB_34	592.0	315.0	0.53	666.03	0.02	0.001	0.0025	0.0001	0.07	0.049	0.004	17.2	1.4	16.1	0.4	170.0	160.0	-7.0	0.8
AFB-00	AFB_81	183.7	129.7	0.71	214.18	0.09	0.011	0.0025	0.0001	0.40	0.270	0.028	89.8	9.9	16.3	0.8	3250.0	170.0	-450.9	7.4
AFB-00	AFB_106	90.8	35.7	0.39	99.19	0.10	0.019	0.0029	0.0002	0.33	0.272	0.046	98.0	17.0	18.8	1.3	3090.0	280.0	-421.3	4.7
AFB-00	AFB_138	153.5	92.2	0.60	175.17	0.16	0.016	0.0030	0.0002	0.56	0.402	0.030	152.0	13.0	19.1	1.1	3840.0	120.0	-695.8	10.2
AFB-00	AFB_39	100.8	57.9	0.57	114.41	0.21	0.029	0.0033	0.0002	0.67	0.415	0.047	186.0	25.0	21.1	1.5	3790.0	240.0	-781.5	6.6
AFB-00	AFB_41	430.0	148.1	0.34	464.80	0.03	0.002	0.0039	0.0001	0.03	0.048	0.004	26.4	2.1	25.2	0.6	120.0	140.0	-4.7	0.6
AFB-00	AFB_16	518.0	353.0	0.68	600.96	0.03	0.002	0.0043	0.0001	0.01	0.048	0.003	29.1	1.6	27.8	0.5	110.0	120.0	-4.6	0.8
AFB-00	AFB_31	227.0	151.0	0.67	262.49	0.03	0.003	0.0043	0.0001	0.06	0.052	0.006	30.6	3.1	27.9	0.8	240.0	200.0	-9.6	0.9
AFB-00	AFB_118	384.0	256.0	0.67	444.16	0.03	0.002	0.0053	0.0001	-0.03	0.045	0.003	32.5	2.1	34.3	0.8	-40.0	130.0	5.1	-0.8
AFB-00	AFB_90	216.0	155.0	0.72	252.43	0.04	0.005	0.0055	0.0002	0.23	0.057	0.006	42.4	4.7	35.0	1.2	470.0	210.0	-21.1	1.6
AFB-00	AFB_58	1210.0	1770.0	1.46	1625.95	0.04	0.002	0.0054	0.0001	0.30	0.051	0.002	37.2	1.7	35.0	0.7	207.0	92.0	-6.3	1.3
AFB-00	AFB_83	220.0	152.0	0.69	255.72	0.04	0.004	0.0055	0.0002	0.06	0.054	0.006	40.4	4.3	35.4	0.9	340.0	220.0	-14.2	1.2
AFB-00	AFB_7	178.1	203.9	1.14	226.02	0.04	0.004	0.0057	0.0002	0.03	0.046	0.005	35.4	3.5	36.9	0.9	20.0	180.0	4.0	-0.4
AFB-00	AFB_36	1528.0	390.0	0.26	1619.65	0.04	0.002	0.0060	0.0001	0.35	0.048	0.002	39.6	1.4	38.5	0.7	121.0	68.0	-3.0	0.8
AFB-00	AFB_87	515.0	142.0	0.28	548.37	0.04	0.002	0.0062	0.0001	0.10	0.047	0.002	40.0	2.0	39.9	0.7	67.0	99.0	-0.2	0.0
AFB-00	AFB_20	283.0	53.7	0.19	295.62	0.04	0.003	0.0064	0.0001	-0.23	0.046	0.004	40.4	3.2	41.4	0.8	30.0	160.0	2.3	-0.3
AFB-00	AFB_65	168.0	73.4	0.44	185.25	0.08	0.008	0.0117	0.0005	0.40	0.051	0.005	79.4	7.6	74.9	3.3	240.0	170.0	-6.0	0.6
AFB-00	AFB_125	235.7	94.4	0.40	257.88	0.08	0.004	0.0121	0.0003	-0.14	0.049	0.003	78.0	4.0	77.5	1.6	120.0	110.0	-0.6	0.1
AFB-00	AFB_54	169.0	55.2	0.33	181.97	0.10	0.006	0.0123	0.0005	0.15	0.059	0.004	94.2	5.7	78.6	2.8	520.0	150.0	-19.8	2.7
AFB-00	AFB_119	468.0	217.0	0.46	519.00	0.11	0.003	0.0168	0.0003	0.43	0.049	0.001	109.0	2.9	107.1	1.6	155.0	64.0	-1.8	0.7
AFB-00	AFB_51	221.7	123.9	0.56	250.82	1.03	0.110	0.0245	0.0009	0.82	0.295	0.026	691.0	58.0	156.1	5.6	3330.0	160.0	-342.7	9.2
AFB-00	AFB_145	245.0	382.0	1.56	334.77	0.18	0.009	0.0257	0.0004	0.06	0.052	0.003	169.6	7.6	163.6	2.7	233.0	97.0	-3.7	0.8
AFB-00	AFB_24	165.3	136.0	0.82	197.26	0.19	0.008	0.0273	0.0005	0.22	0.050	0.002	175.8	6.6	173.5	2.8	198.0	89.0	-1.3	0.3
AFB-00	AFB_126	218.0	173.9	0.80	258.87	0.22	0.008	0.0304	0.0006	0.43	0.051	0.002	199.0	6.4	192.9	4.0	234.0	71.0	-3.2	1.0
AFB-00	AFB_13	585.0	270.0	0.46	648.45	0.27	0.010	0.0367	0.0005	0.47	0.054	0.002	244.7	7.4	232.5	3.1	331.0	66.0	-5.2	1.6
AFB-00	AFB_136	436.0	248.0	0.57	494.28	6.17	0.530	0.0671	0.0048	0.99	0.674	0.018	1970.0	70.0	418.0	29.0	4677.0	42.0	-371.3	22.2
AFB-00	AFB_96	191.0	102.9	0.54	215.18	0.51	0.013	0.0678	0.0010	0.26	0.053	0.001	417.1	8.3	422.6	6.1	341.0	57.0	1.3	-0.7
AFB-00	AFB_48	165.0	123.1	0.75	193.93	0.57	0.018	0.0719	0.0016	0.18	0.059	0.002	460.0	12.0	447.4	9.5	551.0	83.0	-2.8	1.1
AFB-00	AFB_35	245.0	34.0	0.14	252.99	0.56	0.010	0.0727	0.0012	0.47	0.056	0.001	449.7	6.4	452.1	7.1	444.0	44.0	0.5	-0.4
AFB-00	AFB_124	146.0	50.0	0.34	157.75	0.79	0.036	0.0922	0.0033	0.71	0.061	0.002	587.0	20.0	568.0	20.0	621.0	56.0	-3.3	1.0
AFB-00	AFB_61	376.0	197.0	0.52	422.30	1.47	0.120	0.1091	0.0078	0.98	0.097	0.002	902.0	46.0	664.0	45.0	1549.0	37.0	-35.8	5.2

S1 Table. Zircon LA-ICP-MS U-Pb Isotopic Data and Ages for Smith et al., First U-Pb Zircon Ages from Ashfall Fossil Beds (AFB-00) and Grove Lake (GL-00), Nebraska, USA

						Corrected Isotopic Ratios							Ages (Ma)[h]							
Sample ID	Grain #[a]	U[b] [ppm]	Th[b] [ppm]	Th/U	eU[c] [ppm]	$^{207}Pb/^{235}U$[d]	±2s[e]	$^{206}Pb/^{238}U$[d]	±2s[e]	Rho[f]	$^{207}Pb/^{206}Pb$[g]	±2s[e]	$^{207}Pb/^{235}U$	±2s	$^{206}Pb/^{238}U$	±2s	$^{207}Pb/^{206}Pb$	±2s	Disc. %[k]	Wtd. Disc.[l]
AFB-00	AFB_23	116.7	41.8	0.36	126.52	1.66	0.034	0.1650	0.0025	0.36	0.074	0.002	995.0	13.0	984.0	14.0	1033.0	47.0	-1.1	3.5
AFB-00	AFB_22	83.2	81.8	0.98	102.42	1.82	0.058	0.1739	0.0034	0.29	0.076	0.002	1052.0	21.0	1033.0	19.0	1087.0	57.0	-1.8	2.8
AFB-00	AFB_10	232.0	2.1	0.01	232.49	1.79	0.040	0.1770	0.0026	0.47	0.074	0.002	1042.0	15.0	1050.0	14.0	1029.0	43.0	0.8	-1.5
AFB-00	AFB_79	672.0	17.4	0.03	676.09	2.48	0.075	0.1780	0.0058	0.91	0.101	0.002	1265.0	22.0	1054.0	32.0	1635.0	31.0	-20.0	18.2
AFB-00	AFB_11	87.7	61.0	0.70	102.04	1.86	0.038	0.1779	0.0027	0.35	0.075	0.002	1064.0	13.0	1055.0	15.0	1079.0	42.0	-0.9	1.6
AFB-00	AFB_59	319.0	154.1	0.48	355.21	1.96	0.040	0.1831	0.0031	0.68	0.078	0.001	1103.0	14.0	1085.0	17.0	1139.0	35.0	-1.7	3.2
AFB-00	AFB_115	106.3	129.2	1.22	136.66	2.00	0.040	0.1857	0.0026	0.56	0.078	0.002	1114.0	14.0	1098.0	14.0	1153.0	39.0	-1.5	3.9
AFB-00	AFB_121	32.9	18.7	0.57	37.29	1.98	0.085	0.1906	0.0036	0.19	0.078	0.003	1117.0	29.0	1124.0	19.0	1150.0	82.0	0.6	1.4
AFB-00	AFB_64	667.0	186.5	0.28	710.83	3.31	0.140	0.2043	0.0096	0.98	0.118	0.002	1480.0	34.0	1195.0	51.0	1922.0	26.0	-23.8	14.3
AFB-00	AFB_95	34.3	9.7	0.28	36.59	3.16	0.085	0.2332	0.0045	0.37	0.099	0.003	1450.0	21.0	1351.0	24.0	1587.0	53.0	-7.3	9.8
AFB-00	AFB_66	31.4	22.3	0.71	36.64	2.86	0.088	0.2381	0.0047	0.48	0.089	0.003	1384.0	23.0	1376.0	24.0	1404.0	56.0	-0.6	1.2
AFB-00	AFB_151	103.6	40.9	0.39	113.21	3.04	0.078	0.2446	0.0040	0.35	0.091	0.002	1416.0	20.0	1410.0	21.0	1444.0	49.0	-0.4	1.6
AFB-00	AFB_45	163.0	51.6	0.32	175.13	3.49	0.081	0.2693	0.0059	0.79	0.095	0.002	1525.0	18.0	1540.0	29.0	1527.0	34.0	1.0	-0.4
AFB-00	AFB_19	101.3	36.7	0.36	109.92	3.46	0.091	0.2740	0.0048	0.66	0.092	0.002	1516.0	21.0	1561.0	24.0	1466.0	40.0	2.9	-4.0
AFB-00	AFB_25	54.5	21.3	0.39	59.50	3.74	0.079	0.2759	0.0043	0.50	0.099	0.002	1579.0	17.0	1570.0	22.0	1596.0	41.0	-0.6	1.2
AFB-00	AFB_9	420.0	54.3	0.13	432.76	4.20	0.076	0.2933	0.0048	0.72	0.103	0.002	1671.0	15.0	1657.0	24.0	1682.0	28.0	-0.8	1.0
AFB-00	AFB_137	129.0	35.7	0.28	137.39	4.22	0.086	0.2948	0.0061	0.80	0.104	0.002	1675.0	17.0	1664.0	30.0	1699.0	31.0	-0.7	1.2
AFB-00	AFB_146	292.0	41.7	0.14	301.80	4.36	0.110	0.2952	0.0094	0.78	0.107	0.002	1704.0	21.0	1666.0	47.0	1748.0	37.0	-2.3	1.7
AFB-00	AFB_3	311.0	58.4	0.19	324.72	4.22	0.059	0.2966	0.0042	0.80	0.103	0.002	1680.0	12.0	1674.0	21.0	1677.0	26.0	-0.4	0.1
AFB-00	AFB_149	223.9	43.9	0.20	234.22	4.31	0.062	0.3001	0.0040	0.77	0.104	0.001	1694.0	12.0	1691.0	20.0	1705.0	26.0	-0.2	0.7
AFB-00	AFB_120	401.0	341.0	0.85	481.14	4.31	0.066	0.3002	0.0050	0.79	0.105	0.002	1696.0	13.0	1692.0	25.0	1713.0	27.0	-0.2	0.8
AFB-00	AFB_29	417.0	243.0	0.58	474.11	4.43	0.086	0.3012	0.0051	0.82	0.106	0.002	1718.0	16.0	1697.0	25.0	1725.0	27.0	-1.2	1.1
AFB-00	AFB_91	181.0	83.0	0.46	200.51	4.41	0.095	0.3023	0.0056	0.69	0.107	0.002	1713.0	18.0	1705.0	27.0	1741.0	36.0	-0.5	1.3
AFB-00	AFB_2	9.5	4.0	0.42	10.40	11.25	0.640	0.3081	0.0090	0.72	0.266	0.012	2538.0	51.0	1730.0	44.0	3295.0	70.0	-46.7	35.6
AFB-00	AFB_72	269.0	96.5	0.36	291.68	4.62	0.099	0.3101	0.0069	0.89	0.107	0.002	1752.0	18.0	1740.0	34.0	1753.0	28.0	-0.7	0.4
AFB-00	AFB_117	145.3	39.8	0.27	154.65	4.60	0.083	0.3106	0.0062	0.85	0.108	0.002	1749.0	15.0	1743.0	30.0	1757.0	28.0	-0.3	0.5
AFB-00	AFB_50	200.0	61.3	0.31	214.41	4.61	0.110	0.3120	0.0069	0.82	0.108	0.002	1758.0	19.0	1749.0	34.0	1759.0	32.0	-0.5	0.3
AFB-00	AFB_113	152.0	52.0	0.34	164.22	4.58	0.120	0.3137	0.0068	0.79	0.106	0.002	1745.0	21.0	1758.0	33.0	1726.0	40.0	0.7	-1.0
AFB-00	AFB_100	187.0	77.8	0.42	205.28	4.65	0.160	0.3130	0.0110	0.93	0.106	0.002	1760.0	30.0	1765.0	53.0	1733.0	33.0	0.3	-0.6
AFB-00	AFB_97	202.0	56.6	0.28	215.30	4.66	0.100	0.3182	0.0067	0.78	0.106	0.002	1759.0	18.0	1780.0	33.0	1726.0	35.0	1.2	-1.6
AFB-00	AFB_116	144.0	28.3	0.20	150.65	4.77	0.110	0.3217	0.0072	0.76	0.106	0.002	1780.0	19.0	1797.0	35.0	1734.0	34.0	0.9	-1.8
AFB-00	AFB_135	308.0	77.2	0.25	326.14	4.96	0.120	0.3264	0.0060	0.50	0.109	0.002	1811.0	21.0	1823.0	29.0	1776.0	34.0	0.7	-1.6
AFB-00	AFB_15	23.2	15.7	0.68	26.89	5.76	0.120	0.3479	0.0056	0.45	0.121	0.003	1939.0	18.0	1924.0	27.0	1965.0	39.0	-0.8	1.5
AFB-00	AFB_40	98.3	27.9	0.28	104.86	5.70	0.091	0.3556	0.0048	0.70	0.117	0.002	1930.0	14.0	1961.0	23.0	1907.0	27.0	1.6	-2.3
GL-00	GL_79	3,400.0	2,330.0	0.69	3947.55	0.01	0.000	0.0009	0.0000	0.19	0.047	0.003	5.5	0.4	5.5	0.2	110.0	120.0	0.0	0.0
GL-00	GL_27	236.0	140.7	0.60	269.06	0.01	0.003	0.0009	0.0001	0.21	0.071	0.023	9.3	2.5	5.8	0.5	280.0	510.0	-60.3	1.4
GL-00	GL_76	188.5	114.5	0.61	215.41	0.01	0.003	0.0009	0.0001	0.21	0.050	0.025	6.3	2.7	5.9	0.7	-130.0	640.0	-7.5	0.2
GL-00	GL_39	370.0	280.2	0.76	435.85	0.01	0.002	0.0009	0.0001	0.09	0.044	0.012	6.5	1.6	5.9	0.3	70.0	370.0	-10.4	0.4
GL-00	GL_50	452.0	313.1	0.69	525.58	0.01	0.002	0.0009	0.0001	0.03	0.058	0.015	7.2	1.9	5.9	0.4	290.0	460.0	-21.6	0.7
GL-00	GL_8	125.2	75.1	0.60	142.85	0.02	0.004	0.0009	0.0001	0.14	0.199	0.061	19.8	4.4	6.0	0.6	1250.0	710.0	-232.2	3.1
GL-00	GL_40	256.0	162.0	0.63	294.07	0.01	0.003	0.0009	0.0001	0.08	0.067	0.025	7.5	2.6	6.1	0.5	110.0	470.0	-23.6	0.6
GL-00	GL_28	357.0	243.8	0.68	414.29	0.01	0.002	0.0009	0.0001	0.01	0.067	0.014	9.3	1.9	6.1	0.4	580.0	380.0	-53.0	1.7
GL-00	GL_4	227.7	129.3	0.57	258.09	0.01	0.003	0.0009	0.0001	0.07	0.059	0.025	7.3	2.6	6.1	0.5	-120.0	520.0	-19.7	0.5
GL-00	GL_31	393.0	265.0	0.67	455.28	0.01	0.002	0.0009	0.0001	0.03	0.049	0.013	5.6	1.5	6.1	0.4	-80.0	370.0	8.2	-0.3
GL-00	GL_98	217.0	134.0	0.62	248.49	0.01	0.003	0.0009	0.0001	-0.12	0.063	0.035	6.2	3.0	6.1	0.6	-320.0	710.0	-1.6	0.0
GL-00	GL_55	292.9	174.9	0.60	334.00	0.02	0.003	0.0009	0.0001	0.20	0.116	0.021	15.3	2.5	6.1	0.4	1630.0	340.0	-150.4	3.7
GL-00	GL_9	198.6	123.2	0.62	227.55	0.01	0.003	0.0010	0.0001	0.16	0.110	0.039	10.6	3.3	6.1	0.5	160.0	610.0	-72.9	1.4
GL-00	GL_61	463.0	324.0	0.70	539.14	0.01	0.002	0.0010	0.0001	0.08	0.056	0.015	7.0	1.9	6.1	0.4	280.0	420.0	-14.2	0.5
GL-00	GL_49	448.0	250.0	0.56	506.75	0.01	0.002	0.0010	0.0001	0.15	0.054	0.013	6.4	1.7	6.1	0.4	50.0	410.0	-4.2	0.2
GL-00	GL_6	910.0	730.0	0.80	1081.55	0.01	0.002	0.0010	0.0001	-0.02	0.059	0.013	7.5	1.5	6.2	0.4	340.0	340.0	-22.0	0.9
GL-00	GL_84	457.0	309.0	0.68	529.62	0.01	0.002	0.0010	0.0001	0.03	0.061	0.016	7.3	1.9	6.2	0.5	280.0	420.0	-18.7	0.6
GL-00	GL_48	286.0	199.0	0.70	332.77	0.01	0.002	0.0010	0.0001	-0.01	0.060	0.018	7.4	2.2	6.2	0.5	250.0	460.0	-20.1	0.6
GL-00	GL_51	215.2	123.5	0.57	244.22	0.01	0.003	0.0010	0.0001	0.24	0.056	0.025	6.5	3.0	6.2	0.6	110.0	690.0	-5.5	0.1

S1 Table. Zircon LA-ICP-MS U-Pb Isotopic Data and Ages for Smith et al., First U-Pb Zircon Ages from Ashfall Fossil Beds (AFB-00) and Grove Lake (GL-00), Nebraska, USA

						Corrected Isotopic Ratios							Ages (Ma)[h]							
Sample ID	Grain #[a]	U[b] [ppm]	Th[b] [ppm]	Th/U	eU[c] [ppm]	$^{207}Pb/^{235}U$[d]	±2s[e]	$^{206}Pb/^{238}U$[d]	±2s[e]	Rho[f]	$^{207}Pb/^{206}Pb$[g]	±2s[e]	$^{207}Pb/^{235}U$	±2s	$^{206}Pb/^{238}U$	±2s	$^{207}Pb/^{206}Pb$	±2s	Disc. %[k]	Wtd. Disc.[l]
GL-00	GL_20	201.0	123.1	0.61	229.93	0.01	0.002	0.0010	0.0001	0.00	0.065	0.019	8.5	2.4	6.2	0.5	500.0	460.0	-37.8	1.0
GL-00	GL_53	202.0	115.0	0.57	229.03	0.01	0.003	0.0010	0.0001	-0.19	0.073	0.034	7.1	3.2	6.2	0.5	-10.0	630.0	-14.7	0.3
GL-00	GL_81	1,133.0	672.0	0.59	1290.92	0.01	0.001	0.0010	0.0000	0.09	0.050	0.006	6.7	0.8	6.2	0.3	230.0	210.0	-8.2	0.6
GL-00	GL_82	394.0	272.0	0.69	457.92	0.01	0.002	0.0010	0.0001	-0.12	0.052	0.012	6.6	1.5	6.2	0.4	30.0	370.0	-6.3	0.3
GL-00	GL_83	493.0	300.0	0.61	563.50	0.01	0.002	0.0010	0.0001	-0.24	0.058	0.015	6.3	1.6	6.2	0.4	40.0	400.0	-1.3	0.1
GL-00	GL_35	175.0	92.0	0.53	196.62	0.01	0.004	0.0010	0.0001	0.10	0.060	0.043	7.0	4.4	6.2	0.6	-1020.0	870.0	-12.4	0.2
GL-00	GL_65	293.0	193.0	0.66	338.36	0.01	0.003	0.0010	0.0001	-0.12	0.059	0.022	8.5	2.8	6.3	0.5	270.0	580.0	-35.8	0.8
GL-00	GL_102	1,080.0	800.0	0.74	1268.00	0.01	0.001	0.0010	0.0001	0.07	0.047	0.010	6.3	1.2	6.3	0.3	160.0	300.0	-0.6	0.0
GL-00	GL_57	131.3	61.9	0.47	145.85	0.01	0.004	0.0010	0.0001	0.07	0.047	0.044	6.8	3.9	6.3	0.7	-1500.0	1200.0	-8.5	0.1
GL-00	GL_67	324.0	220.0	0.68	375.70	0.01	0.002	0.0010	0.0001	-0.08	0.062	0.017	7.7	2.0	6.3	0.5	270.0	440.0	-22.4	0.7
GL-00	GL_75	252.0	157.4	0.62	288.99	0.01	0.002	0.0010	0.0001	-0.04	0.041	0.018	5.3	2.0	6.3	0.5	-170.0	500.0	16.0	-0.5
GL-00	GL_5	456.0	259.0	0.57	516.87	0.01	0.003	0.0010	0.0001	0.36	0.051	0.020	7.1	2.8	6.4	0.5	170.0	590.0	-11.6	0.3
GL-00	GL_22	335.0	215.0	0.64	385.53	0.01	0.002	0.0010	0.0001	-0.01	0.075	0.019	9.7	2.0	6.4	0.5	510.0	380.0	-52.3	1.7
GL-00	GL_77	328.0	221.9	0.68	380.15	0.01	0.002	0.0010	0.0001	0.07	0.043	0.015	6.3	2.0	6.4	0.4	-110.0	440.0	1.3	0.0
GL-00	GL_96	288.0	178.1	0.62	329.85	0.01	0.003	0.0010	0.0001	-0.04	0.069	0.021	9.7	2.7	6.4	0.5	630.0	500.0	-51.8	1.2
GL-00	GL_13	90.9	59.1	0.65	104.79	0.01	0.008	0.0010	0.0002	0.02	0.140	0.170	8.3	7.9	6.4	0.9	-1500.0	1700.0	-29.7	0.2
GL-00	GL_10	395.0	259.0	0.66	455.87	0.01	0.001	0.0010	0.0001	0.15	0.050	0.011	6.7	1.4	6.4	0.4	20.0	350.0	-4.5	0.2
GL-00	GL_42	272.0	188.0	0.69	316.18	0.01	0.002	0.0010	0.0001	0.18	0.067	0.020	7.7	2.4	6.4	0.4	300.0	480.0	-20.1	0.5
GL-00	GL_100	342.0	251.0	0.73	400.99	0.01	0.002	0.0010	0.0001	0.04	0.048	0.017	7.2	1.9	6.4	0.4	100.0	450.0	-12.3	0.4
GL-00	GL_47	1,550.0	1,024.0	0.66	1790.64	0.01	0.001	0.0010	0.0000	0.18	0.044	0.005	6.2	0.7	6.4	0.3	-20.0	180.0	3.4	-0.3
GL-00	GL_92	375.0	239.0	0.64	431.17	0.01	0.002	0.0010	0.0001	0.07	0.055	0.012	7.4	1.6	6.4	0.4	280.0	360.0	-15.3	0.6
GL-00	GL_15	173.0	99.0	0.57	196.27	0.01	0.003	0.0010	0.0001	0.00	0.081	0.031	9.2	3.2	6.4	0.6	290.0	680.0	-43.1	0.9
GL-00	GL_62	177.0	88.5	0.50	197.80	0.01	0.003	0.0010	0.0001	-0.16	0.096	0.036	10.2	3.3	6.4	0.6	500.0	600.0	-58.6	1.1
GL-00	GL_2	262.0	156.0	0.60	298.66	0.01	0.003	0.0010	0.0001	-0.14	0.073	0.026	8.5	3.0	6.4	0.4	340.0	590.0	-32.0	0.7
GL-00	GL_32	397.0	285.2	0.72	464.02	0.01	0.003	0.0010	0.0001	0.01	0.061	0.021	8.1	2.6	6.4	0.4	-80.0	400.0	-25.8	0.6
GL-00	GL_89	264.0	148.0	0.56	298.78	0.01	0.002	0.0010	0.0001	0.16	0.063	0.023	8.1	2.4	6.4	0.5	-120.0	530.0	-25.8	0.7
GL-00	GL_33	294.5	186.7	0.63	338.37	0.01	0.002	0.0010	0.0001	0.20	0.094	0.017	11.6	2.1	6.5	0.4	940.0	380.0	-79.8	2.5
GL-00	GL_44	316.0	196.0	0.62	362.06	0.01	0.002	0.0010	0.0001	-0.10	0.062	0.021	8.4	2.3	6.5	0.6	600.0	540.0	-30.2	0.8
GL-00	GL_78	352.0	221.0	0.63	403.94	0.01	0.002	0.0010	0.0001	-0.06	0.044	0.017	5.7	2.0	6.5	0.5	-180.0	420.0	11.6	-0.4
GL-00	GL_11	282.0	209.0	0.74	331.12	0.01	0.002	0.0010	0.0001	-0.19	0.065	0.020	8.0	2.2	6.5	0.5	190.0	470.0	-23.8	0.7
GL-00	GL_24	177.0	92.0	0.52	198.62	0.01	0.003	0.0010	0.0001	-0.15	0.079	0.047	7.0	3.1	6.5	0.7	0.0	730.0	-7.9	0.2
GL-00	GL_85	1,256.0	1,200.0	0.96	1538.00	0.01	0.001	0.0010	0.0000	0.11	0.051	0.006	7.1	0.8	6.5	0.3	170.0	180.0	-9.2	0.8
GL-00	GL_21	84.4	51.9	0.61	96.60	0.00	0.006	0.0010	0.0001	0.06	0.075	0.072	4.0	6.5	6.5	0.8	-2100.0	1700.0	38.6	-0.4
GL-00	GL_29	265.0	156.0	0.59	301.66	0.01	0.003	0.0010	0.0001	0.09	0.081	0.025	10.0	2.8	6.5	0.6	490.0	540.0	-53.4	1.2
GL-00	GL_64	88.4	48.0	0.54	99.68	0.01	0.006	0.0010	0.0001	0.08	0.160	0.110	13.7	5.8	6.5	0.9	-700.0	1900.0	-109.5	1.2
GL-00	GL_34	312.3	209.6	0.67	361.56	0.01	0.002	0.0010	0.0001	0.19	0.053	0.013	7.0	1.7	6.6	0.4	140.0	370.0	-6.9	0.3
GL-00	GL_45	237.0	144.0	0.61	270.84	0.01	0.002	0.0010	0.0001	0.16	0.055	0.017	7.2	2.3	6.6	0.5	10.0	460.0	-9.9	0.3
GL-00	GL_71	321.0	170.5	0.53	361.07	0.01	0.003	0.0010	0.0001	-0.10	0.050	0.022	5.8	2.5	6.6	0.6	-340.0	590.0	11.7	-0.3
GL-00	GL_43	226.0	140.0	0.62	258.90	0.01	0.003	0.0010	0.0001	0.13	0.051	0.021	6.9	2.7	6.6	0.5	10.0	570.0	-4.7	0.1
GL-00	GL_59	317.0	206.0	0.65	365.41	0.01	0.003	0.0010	0.0001	0.11	0.067	0.026	8.5	3.2	6.6	0.6	-10.0	620.0	-28.8	0.6
GL-00	GL_66	329.0	212.0	0.64	378.82	0.01	0.002	0.0010	0.0001	0.07	0.078	0.015	10.4	1.9	6.6	0.4	780.0	380.0	-57.6	2.0
GL-00	GL_60	324.9	226.6	0.70	378.15	0.01	0.002	0.0010	0.0001	-0.28	0.063	0.016	7.2	1.8	6.6	0.5	330.0	420.0	-8.8	0.3
GL-00	GL_52	336.0	262.6	0.78	397.71	0.01	0.002	0.0010	0.0001	0.10	0.053	0.013	7.5	1.8	6.7	0.5	190.0	390.0	-12.8	0.5
GL-00	GL_26	305.0	195.0	0.64	350.83	0.01	0.003	0.0010	0.0001	-0.01	0.058	0.026	8.5	2.5	6.7	0.5	-40.0	460.0	-26.9	0.7
GL-00	GL_73	221.8	128.3	0.58	251.95	0.01	0.003	0.0010	0.0001	-0.08	0.057	0.022	6.1	2.7	6.7	0.5	140.0	570.0	9.2	-0.2
GL-00	GL_86	267.0	161.0	0.60	304.84	0.01	0.002	0.0010	0.0001	0.08	0.063	0.021	8.9	2.5	6.7	0.5	-120.0	550.0	-32.0	0.9
GL-00	GL_54	267.0	174.8	0.65	308.08	0.01	0.005	0.0010	0.0001	0.14	0.057	0.032	8.7	4.6	6.8	0.6	-110.0	580.0	-28.7	0.4
GL-00	GL_99	274.0	236.0	0.86	329.46	0.01	0.004	0.0011	0.0001	0.02	0.073	0.026	9.6	3.7	6.8	0.6	420.0	720.0	-41.8	0.8
GL-00	GL_69	280.0	185.0	0.66	323.48	0.01	0.003	0.0011	0.0001	0.19	0.066	0.022	9.0	2.7	6.8	0.6	230.0	590.0	-32.7	0.8
GL-00	GL_18	283.0	199.5	0.70	329.88	0.01	0.002	0.0011	0.0001	-0.07	0.051	0.016	6.6	1.8	6.8	0.4	-50.0	420.0	2.8	-0.1
GL-00	GL_12	274.0	160.8	0.59	311.79	0.01	0.003	0.0011	0.0001	-0.03	0.066	0.029	8.2	2.8	6.8	0.5	-300.0	560.0	-20.1	0.5
GL-00	GL_93	310.0	262.0	0.85	371.57	0.02	0.003	0.0011	0.0001	0.13	0.137	0.022	19.4	3.2	6.8	0.5	2010.0	310.0	-184.0	3.9
GL-00	GL_70	175.6	85.7	0.49	195.74	0.01	0.005	0.0011	0.0001	0.23	0.081	0.037	10.7	4.6	6.9	0.8	600.0	830.0	-56.0	0.8

S1 Table. Zircon LA-ICP-MS U-Pb Isotopic Data and Ages for Smith et al., First U-Pb Zircon Ages from Ashfall Fossil Beds (AFB-00) and Grove Lake (GL-00), Nebraska, USA

						Corrected Isotopic Ratios							Ages (Ma)[h]							
Sample ID	Grain #[a]	U[b] [ppm]	Th[b] [ppm]	Th/U	eU[c] [ppm]	$^{207}Pb/^{235}U$[d]	±2s[e]	$^{206}Pb/^{238}U$[d]	±2s[e]	Rho[f]	$^{207}Pb/^{206}Pb$[g]	±2s[e]	$^{207}Pb/^{235}U$	±2s	$^{206}Pb/^{238}U$	±2s	$^{207}Pb/^{206}Pb$	±2s	Disc. %[k]	Wtd. Disc.[l]
GL-00	GL_1	129.8	44.1	0.34	140.16	0.01	0.005	0.0011	0.0001	0.02	0.100	0.044	10.0	5.3	6.9	0.6	60.0	860.0	-45.6	0.6
GL-00	GL_90	202.0	102.7	0.51	226.13	0.02	0.004	0.0011	0.0001	0.13	0.139	0.031	18.1	4.0	7.0	0.7	1600.0	470.0	-160.1	2.8
GL-00	GL_72	226.0	118.0	0.52	253.73	0.01	0.002	0.0011	0.0001	-0.06	0.064	0.018	7.6	1.9	7.0	0.5	280.0	450.0	-8.6	0.3
GL-00	GL_95	421.0	283.6	0.67	487.65	0.02	0.004	0.0011	0.0001	0.02	0.146	0.029	20.7	4.0	7.1	0.6	1890.0	490.0	-192.4	3.4
GL-00	GL_17	142.0	77.3	0.54	160.17	0.01	0.004	0.0011	0.0001	-0.02	0.120	0.130	12.3	3.9	7.2	0.8	-150.0	970.0	-71.5	1.3
GL-00	GL_91	387.0	269.0	0.70	450.22	0.01	0.003	0.0011	0.0001	0.13	0.069	0.020	9.7	3.0	7.2	0.4	670.0	500.0	-35.3	0.8
GL-00	GL_56	11.8	3.8	0.32	12.70	0.03	0.043	0.0011	0.0006	0.14	-0.270	0.300	32.0	43.0	7.2	3.9	-9300.0	5300.0	-344.4	0.6
GL-00	GL_103	185.0	119.0	0.64	212.97	0.01	0.004	0.0011	0.0001	-0.25	0.058	0.034	7.0	4.1	7.3	0.8	0.0	770.0	4.0	-0.1
GL-00	GL_97	115.4	47.6	0.41	126.59	0.01	0.005	0.0012	0.0001	0.03	0.066	0.046	9.5	4.8	7.5	0.8	-540.0	880.0	-27.5	0.4
GL-00	GL_38	945.0	706.0	0.75	1110.91	0.03	0.004	0.0012	0.0001	0.47	0.173	0.018	27.8	3.4	7.6	0.4	2500.0	180.0	-266.3	5.9
GL-00	GL_88	130.9	65.8	0.50	146.36	0.02	0.005	0.0012	0.0001	0.17	0.139	0.033	22.7	5.1	7.7	0.7	1540.0	530.0	-193.3	2.9
GL-00	GL_63	134.8	95.3	0.71	157.20	0.02	0.006	0.0012	0.0001	0.27	0.161	0.045	23.8	6.2	7.8	0.8	1530.0	640.0	-206.7	2.6
GL-00	GL_94	103.0	50.6	0.49	114.89	0.02	0.009	0.0013	0.0002	0.15	0.153	0.098	16.4	8.7	8.6	1.0	400.0	1100.0	-90.9	0.9
GL-00	GL_46	158.0	103.2	0.65	182.25	0.04	0.006	0.0014	0.0001	-0.08	0.222	0.061	41.8	6.2	8.7	0.8	2480.0	390.0	-380.5	5.3
GL-00	GL_101	191.1	107.0	0.56	216.25	0.06	0.009	0.0014	0.0001	0.58	0.274	0.040	57.4	8.9	8.8	0.8	2930.0	360.0	-551.5	5.5
GL-00	GL_68	759.0	601.0	0.79	900.24	0.04	0.003	0.0014	0.0001	0.16	0.196	0.015	35.3	2.6	8.8	0.4	2750.0	140.0	-299.3	10.2
GL-00	GL_36	111.2	64.6	0.58	126.38	0.04	0.011	0.0014	0.0002	0.05	0.190	0.130	40.0	10.0	9.1	1.1	1760.0	960.0	-339.6	3.1
GL-00	GL_80	132.8	82.8	0.62	152.26	0.05	0.007	0.0015	0.0001	0.24	0.234	0.039	46.1	6.8	9.6	0.8	2690.0	350.0	-379.7	5.4
GL-00	GL_74	166.0	100.9	0.61	189.71	0.06	0.008	0.0015	0.0001	-0.13	0.328	0.048	61.3	7.1	9.7	0.7	3160.0	360.0	-532.0	7.3
GL-00	GL_14	147.8	87.1	0.59	168.27	0.09	0.010	0.0017	0.0001	0.06	0.432	0.053	88.4	8.8	11.1	0.9	3790.0	200.0	-695.0	8.8
GL-00	GL_87	151.2	59.1	0.39	165.09	0.12	0.013	0.0021	0.0002	0.13	0.446	0.063	112.0	12.0	13.2	1.3	3960.0	210.0	-748.5	8.2
GL-00	GL_16	8.1	2.5	0.31	8.65	0.13	0.069	0.0029	0.0012	0.12	-0.050	0.320	114.0	65.0	18.5	7.5	-10200.0	7700.0	-516.2	1.5
GL-00	GL_37	11.2	2.9	0.26	11.86	0.31	0.078	0.0031	0.0009	0.12	0.900	0.430	264.0	55.0	20.0	5.8	1100.0	4500.0	-1220.0	4.4
GL-00	GL_19	235.0	137.6	0.59	267.34	0.03	0.004	0.0041	0.0002	0.12	0.049	0.007	27.0	3.6	26.3	1.1	240.0	250.0	-2.5	0.2
GL-00	GL_30	2.9	0.6	0.19	3.05	0.02	0.220	0.0067	0.0038	-0.12	0.110	0.200	90.0	200.0	42.0	24.0	-7700.0	4200.0	-114.3	0.2
GL-00	GL_23	19.5	13.4	0.69	22.65	2.79	0.310	0.0242	0.0028	0.82	0.822	0.057	1316.0	93.0	153.0	18.0	5000.0	140.0	-760.1	12.5
GL-00	GL_7	23.1	16.0	0.69	26.86	2.71	0.680	0.0287	0.0073	0.90	0.784	0.064	1200.0	160.0	170.0	41.0	4920.0	150.0	-605.9	6.4
GL-00	GL_41	129.8	51.7	0.40	141.95	1.75	0.067	0.1707	0.0052	0.56	0.074	0.002	1026.0	24.0	1015.0	28.0	1035.0	50.0	-1.1	0.7
GL-00	GL_58	77.0	35.9	0.47	85.44	1.92	0.082	0.1812	0.0060	0.52	0.077	0.002	1086.0	29.0	1073.0	33.0	1143.0	57.0	-1.2	2.1
GL-00	GL_25	69.9	34.4	0.49	77.98	2.06	0.077	0.1943	0.0060	0.33	0.077	0.002	1134.0	25.0	1144.0	33.0	1116.0	57.0	0.9	-0.8

[a] Samples are sorted from youngest $^{206}Pb/^{238}U$-age to oldest; Highlighted rows indicate youngest concordant analyses used to calculate depositional ages

[b] U and Th concentrations and Th/U ratios calculated relative to the GJ-1 zircon standard ID-TIMS values using 287 ± 76 ppm for U and 8.4 ± 2.6 ppm for Th (Jackson et al., 2004)

[c] Equivalent U defined by the equation: eU = U ppm + 0.235*Th ppm

[d] Corrected for U-Pb fractionation and background and normalized to the GJ-1 zircon standard ID-TIMS values: $^{207}Pb/^{235}U$ = 0.8093 ± 0.0009 and $^{206}Pb/^{238}U$ = 0.09761 ± 0.00011 (Jackson et al., 2004)

[e] Propagated uncertainty of internal uncertainties (2 SE) and within run reproducibility of GJ-1 (2 SE)

[f] Uncertainty correlation between $^{206}Pb/^{238}U$ and $^{207}Pb/^{235}U$ uncertainties

[g] Corrected for background and Pb isotopic fractionation using the GJ-1 zircon standard ID-TIMS value: $^{207}Pb/^{206}Pb$ = 0.06014 ± 0.00001 (Jackson et al., 2004)

[h] U-Pb ages calculated relative to the weighted mean $^{206}Pb/^{238}U$ age of 600.4 ±0.65 Ma for the GJ-1 zircon reference material (Jackson et al., 2004)

[i] Percent Discordance defined as $(1-(^{207}Pb/^{235}U_{age} / ^{206}Pb/^{238}U_{age}))*100$

[j] Uncertainty weighted age difference defined as $(^{207}Pb/^{235}U_{age} - ^{206}Pb/^{238}U_{age})/(^{207}Pb/^{235}U_{2\sigma\ age\ uncertainty})$ for grains with $^{206}Pb/^{238}U$ ages <900 Ma and $(^{207}Pb/^{206}Pb_{age} - ^{206}Pb/^{238}U_{age})/(^{206}Pb/^{238}U_{2\sigma\ age\ uncertainty})$ for grains with $^{206}Pb/^{238}U$ ages ≥900 Ma

Jackson, S.E., Pearson, N.J., Griffin, W.L., and Belousova, E.A., 2004, The application of laser ablation-inductively coupled plasma-mass spectrometry to in situ U–Pb zircon geochronology: Chemical Geology, v. 211, p. 47-69.

S2 Table. Supervolcano Eruption Data; Smith et al. The first U-Pb zircon ages for the Ashfall Fossil Beds

Age (Ma)	Unit[a]	State	Volcanic Field	Estimated Volume (km^3)[b]	Reference
4.45	Kilgore Tuff	Idaho	Heise	1800	Morgan and McIntosh (2005)
5.51	Conant Creek Tuff	Idaho	Heise	300	Morgan and McIntosh (2005)
6.27	Walcott Tuff	Idaho	Heise	750	Morgan and McIntosh (2005)
6.62	Blacktail Creek Tuff	Idaho	Heise	1500	Morgan and McIntosh (2005)
7.02	Cub River Tuff	Idaho	Picabo	1000	Perkins and Nash (2002)
7.49	Faust Tuff	Idaho	Picabo	1000	Perkins and Nash (2002)
7.90	Rush Valley Tuff	Idaho	Picabo	1000	Perkins and Nash (2002)
8.30	Inkom Tuff	Idaho	Picabo	1000	Perkins and Nash (2002)
9.16	McMullen Creek Tuff	Idaho	Twin Falls	500	Perkins and Nash (2002)
9.41	Lonergan Creek Tuff	Idaho	Twin Falls	500	Perkins and Nash (2002)
9.52	Opal Canyon 6 Tuff	Idaho	Twin Falls	500	Perkins and Nash (2002)
10.25	Rawlins Tuff	Idaho	Twin Falls	500	Perkins and Nash (2002)
10.45	Cougar Point Tuff XV	Idaho	Bruneau-Jarbidge	500	Bonnichsen et al. (2008)
10.75	Cougar Point Tuff XIII	Idaho	Bruneau-Jarbidge	1000	Bonnichsen et al. (2008)
11.22	Cougar Point Tuff XI	Idaho	Bruneau-Jarbidge	1000	Bonnichsen et al. (2008)
11.59	Cougar Point Tuff IX	Idaho	Bruneau-Jarbidge	500	Bonnichsen et al. (2008)
11.81	Cougar Point Tuff VII	Idaho	Bruneau-Jarbidge	750	Bonnichsen et al. (2008)
11.93	Ibex Hollow Tuff	Idaho	Bruneau-Jarbidge	500	Perkins and Nash (2002)
12.67	Cougar Point Tuff III	Idaho	Bruneau-Jarbidge	500	Bonnichsen et al. (2008)
13.5	Hurlbut Tuff	Idaho	Owyhee-Humboldt	950	Perkins and Nash (2002)
13.80	Swisher Mountain Tuff	Idaho	Owyhee-Humboldt	1430	Ekren et al. (1984)

[a] Ash-flow tuffs geochemically correlated with airfall deposits on the Great Plains (from Figure 5 in Perkins and Nash, 2002).

[b] When possible, eruption volumes are from estimated ashfall volumes reported in cited references.

Bonnichsen B, Leeman WP, Honjo N, McIntosh WC, Godchaux MM (2008) Miocene silicic volcanism in southwestern Idaho: Geochronology, geochemistry, and evolution of the central Snake River Plain. Bulletin of Volcanology 70: 315–342.

Ekren EB, McIntyre DH, Bennett EH (1984) High-temperature, large-volume, lavalike ash-flow tuffs without calderas in southwestern Idaho. U.S. Geological Survey Professional Paper 1272: 76 p.

Morgan L A, McIntosh W C (2005) Timing and development of the Heise volcanic field, Snake River Plain, Idaho, western USA. Geological Society of America, Bulletin 117: 288-306.

Perkins, M.E., and Nash, B.P., 2002, Explosive silicic volcanism of the Yellowstone Hotspot: the ash fall tuff record: Geological Society of America, Bulletin, v. 114, p. 367–381.